SUPPORTING INFORMATION

Upcycling atmospheric CO_2 to polyhydroxyalkanoates via sequential chemo-biocatalytic processes

Manuel Bruch[1,2†], Julian E. Sanchez-Velandia[3†], Jhonatan Rodríguez-Pereira[4,5], Michelle Rich[6], Nicole Pearcy[6], Tanja Narančić[1,2], Eduardo Garcia-Verdugo[3], Victor Sans[7], Kevin O'Connor[1,2*], Marcileia Zanatta[7,8*]

1. School of Biomolecular and Biomedical Sciences, University College Dublin, Dublin, Ireland
2. BiOrbic, Bioeconomy SFI Research Centre, Dublin, Ireland
3. Departamento de Quimica Inorganica y Organica, Universitat Jaume I, Avda Sos Baynat, s/n, 12071 Castelló de la Plana, Spain
4. Center of Materials and Nanotechnologies, Faculty of Chemical Technology, University of Pardubice, Nam. Cs. Legii 565, 53002 Pardubice, Czech Republic
5. Central European Institute of Technology, Brno University of Technology, Purkynova 123, 61200 Brno, Czech Republic
6. BBSRC/EPSRC Synthetic Biology Research Centre (SBRC), University of Nottingham, University Park, Nottingham, NG7 2RD, United Kingdom
7. Institute of Advanced Materials (INAM), Universitat Jaume I (UJI), Avda Sos Baynat, s/n, 12071 Castelló de la Plana, Spain
8. Departament de Química Física i Analítica, Universitat Jaume I, Av. Sos Baynat s/n, 12071 Castelló de la Plana, Spain

† These authors contributed equally to the work.

* zanatta@uji.es, kevin.oconnor@ucd.ie

Contents

S1. Materials and Reagents

All reagents and solvents used were commercially available: tetrabutylammonium hydroxide (1 mol.L^{-1} in methanol, Sigma Aldrich). Amberlite IR-120 (in H+ form).). All the solvents were used as received from VWR Chemicals. H_2 gas was supplied by Air Liquide with purity above 99.998 % and atmospheric air containing 0.04% of CO_2. Merrifield resin (5.5 meq/g Cl) and formaldehyde were provided by Aldrich. $RuCl_3.3h_2O$ was purchased from Indagoo. $SOCl_2$ was provided by Across Organics. Both KOtBu and H-imidazole were purchased from Fluka Analytical.

S2. Methods

S2.1 Catalyst characterization

FTIR spectra were obtained by using a spectrometer (JASCOFT/IR-6200) equipped with an ATR (MIRacle single-reflection ATR diamond/ZnSe) accessory at 4cm^{-1} resolution (4000–600cm^{-1} spectral range). To determine the surface chemical composition of some selected heterogeneous samples, X-ray photoelectronic spectroscopy (XPS) was carried out (ESCA 2SR, Scienta-Omicron) with a monochromatic Al Kα X-ray source (1486.7 eV). The charge was controlled with the charge neutralizer (CN-10) operated at 5μA and 1eV. The overall binding energy was referenced based on the adventitious carbon (284.8 eV); on the other hand, quantitative data was performed by using CasaXPS software using the elemental sensitivity factors provided by the manufacturer. Ru 3d spectra were fitted with Shirley-type background and asymmetric Lorentzian functions LA(1.1,2.5,80). All the other spectra were fitted with Shirley-type background and mixed Gaussian-Lorentzian functions GL (30). Also, the area ratio and binding energy distance constraints between the spin–orbit splitting of Ru 3d (Ru $3d_{5/2}$ and Ru $3d_{3/2}$), 3:2 and 4.20 eV, Cl 2p (Cl $2p_{3/2}$ and Cl $2p_{1/2}$), 2:1 and 1.60 eV and K 2p (K $2p_{3/2}$ and K $2p_{1/2}$), 2:1 and 2.8 eV, respectively, were considered. ^{1}H NMR experiments were performed by using a Varian INOVA 300 (300 MHz) spectrometer. Chemical shifts are given in δ values relative to trimethylsilane (TMS) and the coupling constants (J) are given in Hz.

S2.2 Strains

All experiments in this study were performed either with the wildtype (WT) strain *C. necator* H16 (DSM 428) or with the adapted ALE strain.

S2.3 Media

Luria-Bertani (LB) medium was used as a rich medium for primary precultures and plates. Premixed Lennox formulation was used at a concentration of 20 g/L. For inoculum and main cultures, J minimal medium (J-MM) was used as described by Li et al. [1] (0.5 g/L KH_2PO_4, 6.8 g/L Na_2HPO_4 x 12 H_2O, 0.2 g/L $MgSO_4$ x 7 H_2O, 0.02 g/L $FeSO_4$ x 7 H_2O, 4 mg/L $CaCl_2$ x 2 H_2O, 0.1 mg/L thiamine hydrochloride and 1 ml/L adapted SL7 metals solution (1 % (v/v) 5 mol/L HCl (aq), 2.04 g/L $FeCl_3$ x 6 H_2O, 0.19 g/L $CoCl_2$ x 6 H_2O, 0.1 g/L $MnCl_2$ x 4 H_2O, 0.07 g/L $ZnCl_2$, 0.062 g/L H_3BO_3, 0.036 g/L Na2MoO_4 x 2 H_2O, 0.025 g/L $NiCl_2$ x 6 H_2O, and 0.017 g/L $CuCl_2$ x 2 H_2O)). In cases where carbon was the growth limiting substrate, 1 g/L $(NH_4)_2SO_4$ was used as the nitrogen source. The medium was supplemented with the desired carbon source to the final working concentration. In case of cultivation in a non-pH-controlled system like flasks or plates in combination with an organic acid like formic acid as the carbon source, 0.2 mol/L MOPS was added for increased buffering capacity. Medium pH was adjusted to 7.2. For solid media cultivation, 1.5 % (w/v) agar was added to the respective medium.

S2.4 Cultivation in Baffled Shake Flasks

To monitor and measure growth at small scale, individual colonies of *C. necator* were picked from an agar plate to ensure genetic homogeneity within the culture. A first preculture was performed in 10 ml medium (LB in case of the WT and J-MM with 80 mM of carbon (C-mM) from the desired carbon source for adapted strains) in sterile 50 ml tubes at 30 °C and 200 rpm in New Brunswick Innova® 44 shakers (Eppendorf, Hamburg, Germany). On LB medium, the WT achieved sufficient biomass after 15 – 24 h while the adapted strains required 48 – 72 h on J-MM to grow to a sufficient biomass. After that time, a secondary preculture was grown for both the WT and ALE strains in 25 ml of J-MM with 80 C-mM of the desired carbon source in 250 ml baffled flasks with the same shaking conditions as noted above. This secondary culture was inoculated from the primary culture to a starting optical density at 600 nm (OD_{600}) of 0.05. After incubation, the secondary culture was used to inoculate the main culture to the same starting OD_{600}. When flasks were used, the final volume of culture was kept between one tenth and one fifth of the total volume of the flask to ensure sufficient oxygenation of the organisms.

S2.5 Cultivation in Bioreactors

All bioreactor cultivations were carried out in stirred tank vessels of the F0-Baby model by Bionet (Fuente Álamo (Murcia), Spain) at a working volume of 1 L. The process was controlled and monitored using the company's ROSITA software.

S2.5.1 Batch Cultivations

During the reactor setup, the reactor was assembled and filled with 880 ml of a 1.36x concentrated solution of $(NH_4)SO_4$, KH_2PO_4, Na_2HPO_4 x 12 H_2O and carbon source for J-MM. To this 880 ml solution 100 ml of a 10x solution containing all the required salts as detailed above was added. Precultures were performed as described above, the last of which took place in 100 ml J-MM in 1 L baffled shake flasks. This culture was pelleted, and the pellet resuspended in phosphate buffer to an OD_{600} of 2.5, 20 ml of which were used to inoculate the reactor. The initial stirrer speed was set to 500 rpm and gas flow to 1 L_{gas}/L_{liquid}/min. Dissolved oxygen (DO) in the vessel was regulated at a minimum of 20 % by an increase of stirring speed followed by an increase in air flow up to 1500 rpm and 3 L_{gas}/L_{liquid}/min respectively. pH was controlled at 7.2 by feeding 4 M KOH and 15 % (v/v) H_2SO_4. Furthermore, CO_2 and O_2 content in the exhausted air were analysed via a bBreath module from Bionet. Samples were taken in regular intervals to be analysed for biomass content and carbon and nitrogen concentration estimation.

S2.5.3 Continuous Cultivation

For continuous cultivations, the bioreactor was set up as described in S2.5.1 Batch Cultivations. It was operated in batch for 12 h before the pumps were activated. The feed was controlled manually by setting the pump rate [ml/min] to match the desired dilution rate [h^{-1}]. Spent medium (bleed) was harvested by controlling the weight of the bioreactor using a Defender™ 5000 scale (Ohaus, Parsippany, NJ, USA) so that over time it would remain constant despite the continuous feed and pH control. The fed medium was J-MM, with concentrations of the desired carbon source and $(NH_4)_2SO_4$ matching the conditions desired in each experiment. Samples were taken directly from the bioreactor rather than from the bleed line with the weight-controlled bleed ensuring that the full volume would fill up in a temporary fed-batch process before re-entering true continuous operation.

S2.5.4 Adaptive Laboratory Evolution (ALE)

ALE of *C. necator* H16 was performed in continuous cultivation with stepwise increasing dilution rates. The feed medium composition remained constant over the entirety of the experiment, at 80 mM formic acid and 1 g/L $(NH_4)_2SO_4$. The initial dilution rate was set to

0.05 h^{-1}. The rate was maintained before each increase for at least five retention times. Samples for offline biomass and substrate monitoring were taken daily. The dilution rate was increased until it exceeded the initially determined μ_{max} of the WT. At each timepoint of increased dilution rates as well as at the very end, a sample was taken aseptically from the reactor to prepare a glycerol stock (40 % (v/v) glycerol) for later analysis.

S2.6 Screening of the ALE Experiment

The final glycerol stock taken from the ALE experiment was recovered by first resuspending some of the frozen sample in 10 ml J-MM with 80 mM formic acid and 1 g/L $(NH_4)_2SO_4$ in a 50 ml falcon tube for five days at 30 °C and 200 rpm in the Innova® 44 shaker. Once the suspension reached an OD_{600} of ~0.5, 100 µl of a 10^{-8} diluted solution were plated on a J-MM agar plate with the same nutrient composition as the liquid medium. 43 individual colonies were then picked to be screened in the BioLector. As a control, a biological triplicate of the WT strain was included. The medium composition for the precultures and final screen was the same as in the strain recovery. The measured BioLector signal was converted into cell dry weight (CDW) [g/L]. From the observed growth curves, growth rates were calculated with a sliding window algorithm in MATLAB and a window size of 20 data points, equating to 3.3 h of growth. The five strains with the highest maximal growth rates were chosen for further analysis.

The second round of screening was conducted in 50 ml of J-MM with the same composition as before in 250 ml baffled flasks and biological triplicates. Samples for biomass and formic acid concentration estimation were taken in regular intervals and the growth rates for each strain calculated as before.

S2.7 Genome Sequencing

Genomic DNA was extracted using a GeneJet Genomic DNA Purification Kit (Thermo Fisher Scientific, Waltham, MA, USA). Additionally, in order to capture sufficient material of the megaplasmid pHG1, a midiprep was carried out with a Plasmid Midi Kit (Qiagen, Hilden, Germany).

Genome sequencing of the *C. necator* H16 WT as well as the evolved strain was performed by Eurofins Genomics Limited (Ebersberg, Germany) through their INVIEW Resequencing of Bacteria service with an additional data package for higher coverage. The resulting reads were mapped using Geneious Prime (Biomatters, Auckland, New Zealand) to the reference genome sequenced by Little et al. [2]. Reads were trimmed using the BBDuk plugin before alignment against the published sequences of chromosome 1, chromosome 2 and pHG1.

S2.8 Test for Presence of Megaplasmid pHG1

The presence of the megaplasmid pHG1 was determined via polymerase chain reaction (PCR). Primers for the amplification of a DNA fragment containing the RepB family plasmid replication initiator protein CDS were designed in Geneious Prime (Forward: CTGGCGTTGAGTTTGTGGTG, “pHG1_pF”; Reverse: CATACAGGCCGCACAATTCG, “pHG1_pR”).

PCRs were conducted in 50 µl total volume, following the Q5® High-Fidelity DNA Polymerase protocol by New England Biolabs (Ipswich, Massachusetts, USA). The reaction was carried out with two different types of templates for each organism: a) extracted plasmid (extraction was performed according to the QIAGEN® Plasmid Purification Handbook for Very Low-Copy Plasmids); b) freshly picked colonies from each strain as a whole-cell template.

PCR products were visualised via agarose gel electrophoresis, using a 1 % (w/v) agarose gel and SafeView™ classic stain (Applied Biological Materials Inc., Richmond, BC, Canada).

S2.9 Cell Dry Weight Estimation

Biomass during each cultivation was monitored by measurement of OD_{600}. For conversion to cell dry weight (CDW [g/L]), a conversion factor was calculated. For this purpose, *C. necator* H16 was grown in flasks in biological triplicates on formic acid and sodium gluconate respectively to a final OD_{600} between 0.5 and 0.6. 50 ml of each culture were vacuum filtered, washed with ddH_2O and then dried for 24 h on pre-weighed filter membranes. From the weight of the dried pellets, known final OD_{600} and known filtered volume, the conversion factors for each carbon source were estimated. In case freeze-dried samples were used for an experiment, the weight of the pellets was determined directly rather than calculated from OD_{600} with the respective factor.

S2.10 Analytical procedures

S2.10.1 Formic Acid Measurement

Samples from cultivations were pelleted and the supernatant used for estimation of residual substrate concentrations. Formic acid was measured via High Pressure Liquid Chromatography (HPLC) in an Aminex HPX-87 H ion exclusion column (Bio-Rad, Hercules, California, USA). 0.0142 M H_2SO_4 was used as the mobile phase at a pressure of 4.3 MPa and 40 °C. Detection took place in a refractive index (RI) detector (RID-10 A, Shimadzu, Kyoto, Japan) in a SIL-20ACHT HPLC machine (Shimadzu).

S2.10.2 Nitrogen Measurement

Nitrogen in the sample supernatant was analysed via an Indophenol colorimetric assay, following the protocol of Scheiner et al. [3]. Samples were diluted appropriately with ddH_2O prior to analysis to fall within the detection limit. The assay was performed in the wells of a 96-well plate with a final reaction volume of 200 µl.

S2.10.3 Polyhydroxybutyrate Estimation

The intracellular PHB content of *C. necator* cells was estimated via gas chromatography (GC) measurement after subjecting freeze-dried cells to acidic methanolysis [4, 5]. The resulting monomers were quantified in a Hewlett-Packard 6890N chromatograph (Agilent Technologies, Santa Clara, California, USA) on a BP21 capillary column (25 m by 0.25 mm, 0.32 µm film thickness, Trajan Scientific and Medical, Ringwood, Victoria, Australia) and a flame ionisation (FI) detector. From the resulting peak areas, PHB content as a percentage of CDW was calculated, as well as PHB titer (g/L) and productivity (g/L/h) in the originating experiment.

S2.11 Proteomics analysis

For proteomics analysis of *C. necator* strains under different growth conditions, biological duplicate samples were collected and further split into two technical replicates each. Samples were handed to the Proteomics Core facilities of University College Dublin. There, samples were run in a Thermo Scientific Q Exactive workflow with the Thermo Scientific Ultimate 3000 RSLCnano chromatography system (electrospray ionisation liquid chromatography-mass spectrometry (ESI LC-MS), using a quadrupole with high resolution high mass accuracy (HRAM) by Orbitrap). Peaks were analysed in these facilities using MaxQuant software.

S2.11.1 Sample Preparation

Following collection from the bioreactor, samples were pelleted and subsequently lysed with 8 M urea in 0.1 M ammonium bicarbonate. Total protein amounts were quantified via a Bradford assay in 96-well plates. Samples were reduced with dithiothreitol and alkylated with iodoacetamide before digestion with trypsin over night at 37 °C. The following day, the reaction was stopped using trifluoroacetic acid, vacuum-dried and de-salted using C-18 ZipTips. Peptides were resuspended in 15 µl 0.1 % formic acid and the final total peptide concentration estimated on a NanoDrop.

S2.11.2 Data Analysis

Following peak identification in MaxQuant, data were loaded into the Perseus software. Rows were filtered for reverse identifications, potential contaminants and those only identified by site and normalised using log2() transformation. The matrix was split based on a minimum occurrence of two peaks for a protein per strain to generate one submatrix with proteins occurring in *C. necator* H16 as well as the adapted strain and one with proteins that potentially only occur in either. The resulting matrices were further depleted of proteins that occurred less than once in all of the replicates observed. Finally, the matrix containing data for proteins expressed only in one of the tested strains was separated into two, one containing proteins only expressed in the WT strain and one in the adapted strain. Data imputation was performed with a width of 0.8 and a down shift of 1.8.

All created matrices were exported and loaded into GraphPad PRISM for further statistical analysis. For each, a two-way ANOVA with a post-hoc Šidák test were performed to identify statistically significantly differentially expressed proteins across the tested conditions. Finally, python was used to assign pathway functionalities to each protein based on UniProt and KEGG annotations for graphical representation.

S2.11.3 Resource Balance Analysis

Resource Balance analysis (RBA) was performed in python using the RBApy toolbox as described by the authors of **¡Error! Referencia de hipervínculo no válida.** and the model created by Jahn *et al.* [6]. As input parameters, the salt concentrations in J-MM for each of the investigated conditions were imported into the model. Using python, the resulting proteome predictions were correlated with the measured data.

S2.12 Growth and PHB Production of an adapted C. necator *strain on Tetrabutylammonium Formate*

For assessing growth of *C. necator* ALE26 on tetrabutylammonium formate ($TBA.HCO_2$), the organism was grown in various conditions in the BioLector 1. Cultivation in biological triplicates was performed in J-MM containing 200 mM MOPS on 2.5, 5.0, 10.0, 20.0, 40.0 and 80.0 mM $TBA.HCO_2$ as the sole carbon source, as well as 80 mM free formic acid supplemented with either none, 2.5, 5.0, 10.0 or 20 mM $TBA.HCO_2$ and 80 C-mM sodium gluconate supplemented with either none, 2.5, 10.0 or 20.0 mM $TBA.HCO_2$. The inoculum was grown in biological triplicates in J minimal medium with 80 mM formic acid in shake flasks as described above.

To test PHB accumulation in *C. necator* ALE26 from TBA.HCO_2 as the sole carbon source, triplicate precultures of the organism were grown in J-MM with 200 mM MOPS and 40 mM TBA.HCO_2 as the sole carbon source for five days. The cultures were spun down and the pellet resuspended in J-MM with 10,000x reduced phosphate, 200 mM MOPS and 40 mM TBA.HCO_2. For non-phosphate limited growth, the organism was cultivated in 50 ml J-MM with the same composition as the preculture medium. In parallel, a triplicate was cultivated in 200 ml J-MM with the same composition as the resuspension medium for phosphate limited growth. All flasks were harvested after eight days of uninterrupted cultivation, the pellets freeze dried and their PHB content determined via GC.

S3. Synthesis and Characterisation of all immobilised NHC ligands and related complexes.

S3.1 Experimental procedure:

Synthesis of NHC-ligand

Synthesis of polymer **2**: A Merrifield resin (5 g, 1.1 mmol Cl/g, 1% DVB, 5.5 mmol) was introduced in a flask and suspended in DMF (50 mL). Then, diethanolamine (2 mL, 34 mmol) was added. The system was heated at 70 °C for 1 h. The polymer was then filtered and washed with DMF, DMF:MeOH (1:1), MeOH and CH_2Cl_2.

Synthesis of polymer **3**. The polymer **2** (1.53 g, 6.1 mmol) was suspended in CH_2Cl_2 (40 mL). Then, $SOCl_2$ (3 mL, 41.3 mmol) was diluted in CH_2C_{l2} (20 mL) and added dropwise to the suspension at 0 °C. When the addition was complete, the reaction was stirred for 30 min at room temperature, and then heated 4 h at 50 °C, and finally it was left overnight at room temperature. The polymer was then filtered and washed with THF, THF:H_2O (Na_2CO_3), H_2O, H_2O:THF (1:1), THF, MeOH and CH_2Cl_2 and vacuum dried.

Synthesis of supported NHC-ligand **4a** (SILP-bis-(1-mesityl-1H-imidazole): The polymer **3** was introduced in a flask and suspended in a solution of an excess of 1-mesityl-1H-imidazole (0.58g, 3.1 mmol) in DMF (25 mL). The reaction was then heated for 24 h at 80° C. After this period, the polymer was filtered and washed with DMF and MeOH and vacuum dried overnight at 50°C. FT-IR-ATR (cm^{-1}): 3381, 3018, 2918, 1695, 1660, 1601, 1572, 1551, 1510, 1450, 1427, 1360, 1308, 1265, 1213, 1164, 1109, 1068, 1043, 1020, 970, 943, 908, 825, 725, 654, 604. Elemental analysis found: %N 6.2 %C 59.4 %H 6.4; loading 1.0 meq/g.

Synthesis of supported NHC-ligand **4b**. The same procedure as for the preparation of **4a**, employing 1-(2,6-diisopropylphenyl)-1H-imidazole FT-IR-ATR (cm^{-1}): 2964, 2925, 2845, 1670, 1604, 1573, 1541, 1507, 1446, 1420, 1388, 1366, 1307, 1256, 1212, 1178, 1107, 1060, 1035, 1018, 961, 944, 823, 724, 657. Elemental analysis found: %N 4.7 %C 63.9 %H 6.3; loading 1.0 meq/g.

Synthesis of supported Ru-NHC complex (**C1**): Polymer **4a** (50mg, 0.10 mmol) and BuOtK (97 mg,0.86 mmol) were added to a Schlenk tube and then the vessel was evacuated and flushed with nitrogen three times. Afterwards, dry THF (30 mL) was added, and the mixture was constantly stirred for 2 h under N_2 atmosphere. Then, 63mg (0.23 mmol) of $[Ru(CO)_2Cl_2]_n$ was added and the solution was left under stirring for 24 h at room

temperature. After this, the polymer was filtered off and washed with THF (5x10 mL) and CH_2Cl_2 (5x10 mL). Finally, the polymer was dried under vacuum at 60 °C.

The Ru content was determined by ICP–MS. A known amount of the polymer containing palladium (ca. 10 mg.) was introduced in a round-bottomed flask and suspended in 20 mL of a mixture HCl:HNO_3 (1:1). The flask was heated at 100 °C for 4 h. Then the polymer was filtered and washed with 10 mL of H_2O. The filtered phases were combined and analyzed by ICP–MS. FT-IR-ATR (cm^{-1}): 2919, 2854, 2049, 1972, 1667, 1605, 1571, 1541, 1507, 1447, 1422, 1360, 1307, 1265, 1212, 1167, 1114, 1063, 1018, 946, 910, 827, 719, 674. Elemental analysis found: %N 4.7 %C 61.8 %H 5.8; loading 0.68 mmol/g. Ru loading 0.170 mmol/g

Synthesis of supported Ru-NHC complex (**C2**): the same procedure as for the preparation of **C1**, employing [Ru(bis-allyl)Cl_2]$_2$ as Ru source FT-IR-ATR (cm^{-1}): 2914, 2850, 2081, 1938, 1651, 1539, 1416, 1376, 1210, 1157, 1104, 1018, 967, 896, 826, 667. Elemental analysis found: %N 4.8 %C 60.4 %H 7.3; loading 0.68 mmol/g. Ru loading 0.510 mmol/g

Synthesis of supported Ru-NHC complex (**C3**): the same procedure as for the preparation of **C1**, employing [Ru(*p*-cymene)Cl_2]$_2$ as Ru source. FT-IR-ATR (cm^{-1}): 2923, 2851, 1695, 1664, 1574, 1561, 1540, 1508, 1449, 1422, 1357, 1307, 1271, 1212, 1174, 1109, 1061, 1018, 974, 947, 918, 827, 727, 663, 627. Elemental analysis found: %N 4.6 %C 61.2 %H 6.3 loading 0.66 mmol/g. Ru loading 0.296 mmol/g

Synthesis of supported Ru-NHC complex (**C4**): the same procedure as for the preparation of **C1**, employing the supported NHC-ligand 4b and [Ru(bis-allyl)Cl_2]$_2$ as Ru source. FT-IR-ATR (cm^{-1}): 3010, 2921, 2847, 2119, 1929, 1661, 1606, 1510, 1442, 1362, 1305, 1258, 1208, 1180, 1111, 1059, 1015, 945, 825, 733, 654. Elemental analysis found %N 4.8 %C 60.4 %H 7.3 loading 0.68 mmol/g. Ru loading 0.450 mmol/g

Synthesis of supported Ru-NHC complex (**C5**): the same procedure as for the preparation of **C1**, employing the supported NHC-ligand 4b. FT-IR-ATR (cm^{-1}): 2922, 2846, 2046, 1969, 1666, 1605, 1570, 1554, 1540, 1510, 1448, 1421, 1362, 1301, 1249, 1214, 1168, 1111, 1063, 1039, 1013, 970. 937, 829, 731, 649. Elemental analysis found: %N 4.8 %C 59.8 %H 6.5 loading 0.68 mmol/g. Ru loading 0.169 mmol/g

S3.2 Chemical structures: Figure S1 illustrates the three-step solid-phase synthetic strategy employed for the synthesis of immobilized NHC ligands. These ligands were

subsequently used to form the related organometallic complexes utilizing three different Ru precursors: $[RuCl_2(CO)_2]_n$, $[Ru(bis\text{-}allyl)Cl_2]_2$, and $[RuCl_2\text{-}(p\text{-cymene})]_2$.

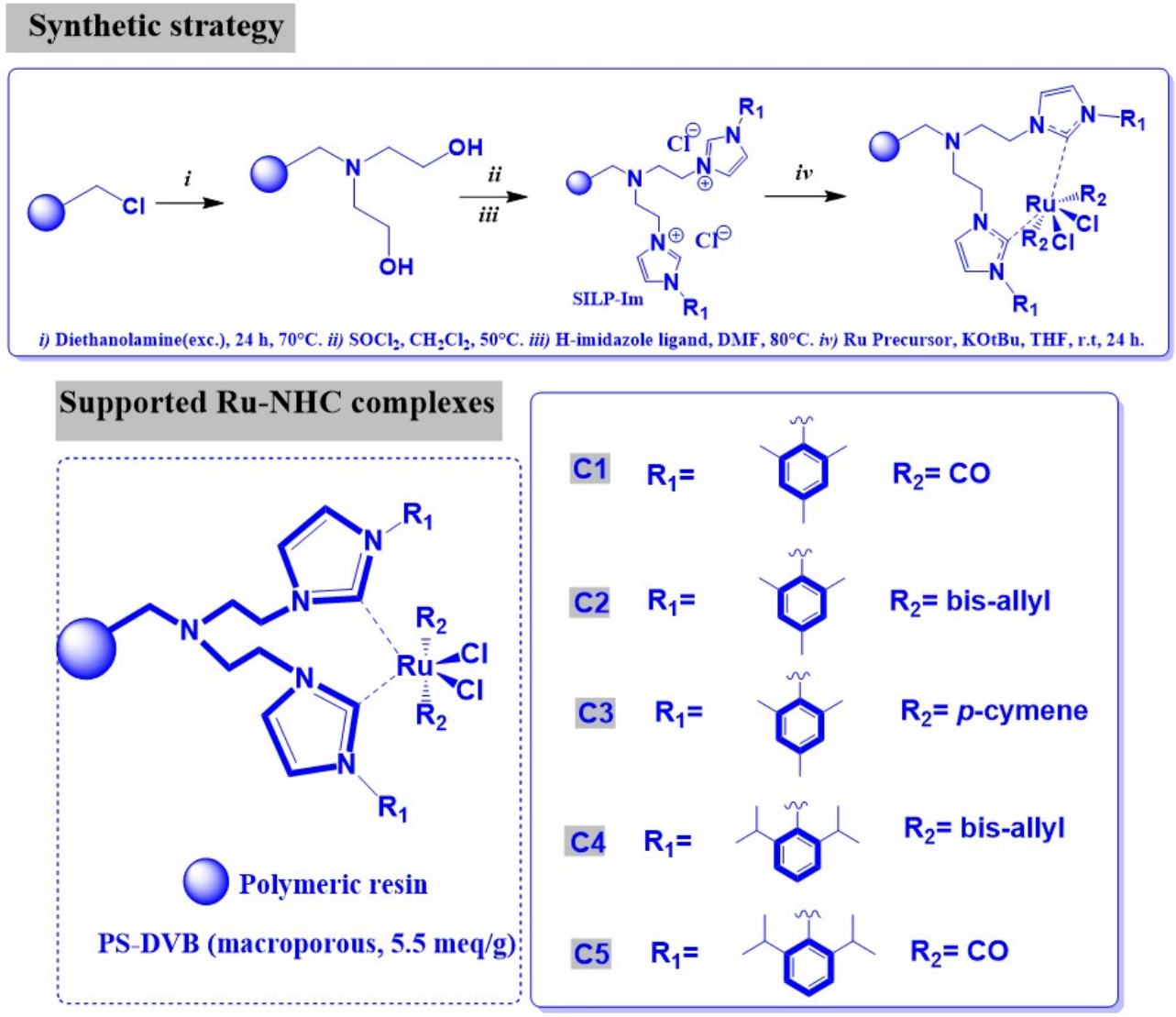

Figure S1. Synthetic strategy and schematic representation of the heterogeneous catalysts.

S3.3. FT-IR-ATR of all the catalyst

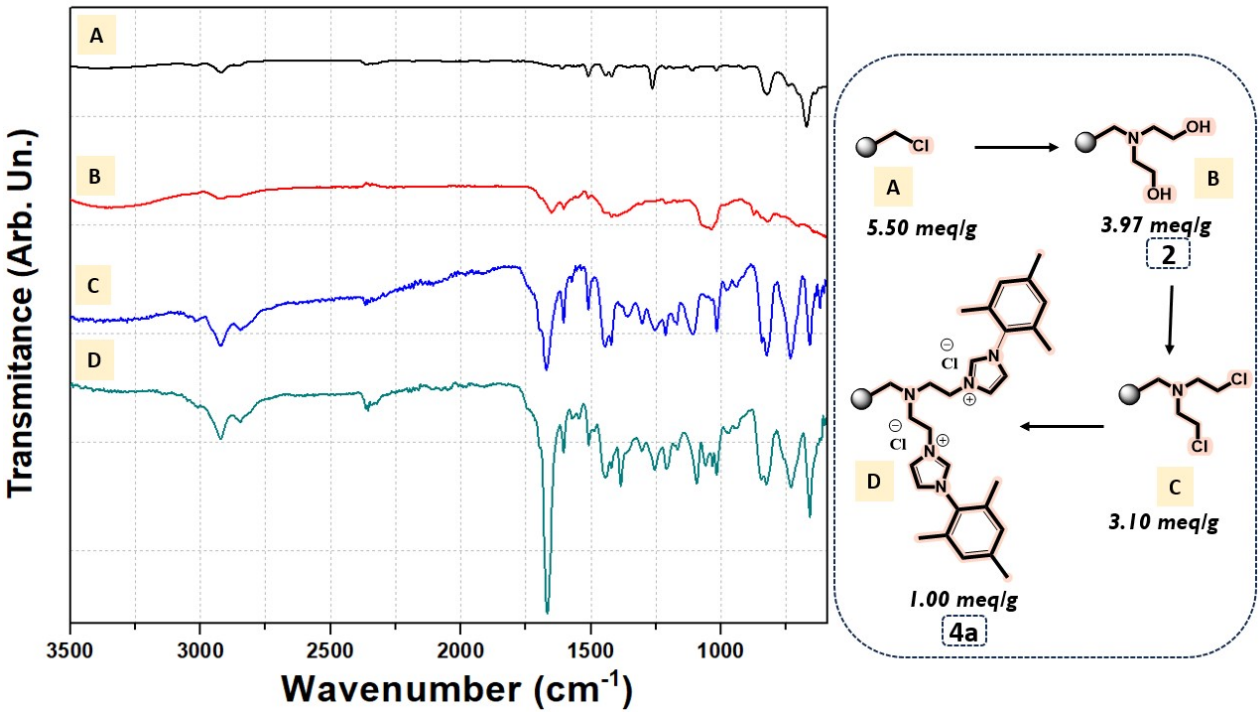

Figure S2. FTIR-ATR spectra for the intermediates used for the synthesis of supported NHC ligand subsequently used to prepare the catalysts C1 and C4.

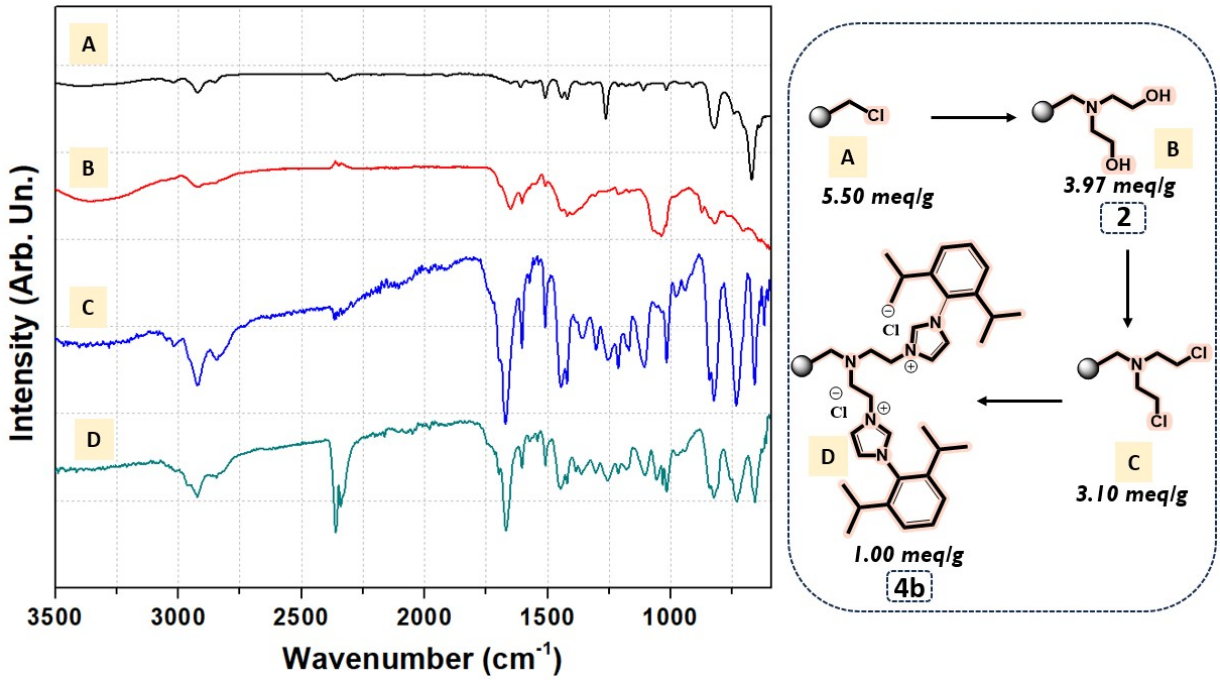

Figure S3. FTIR-ATR spectra for the intermediates used for the synthesis of supported NHC ligand subsequently used to prepare the catalysts C2, C3 and C5.

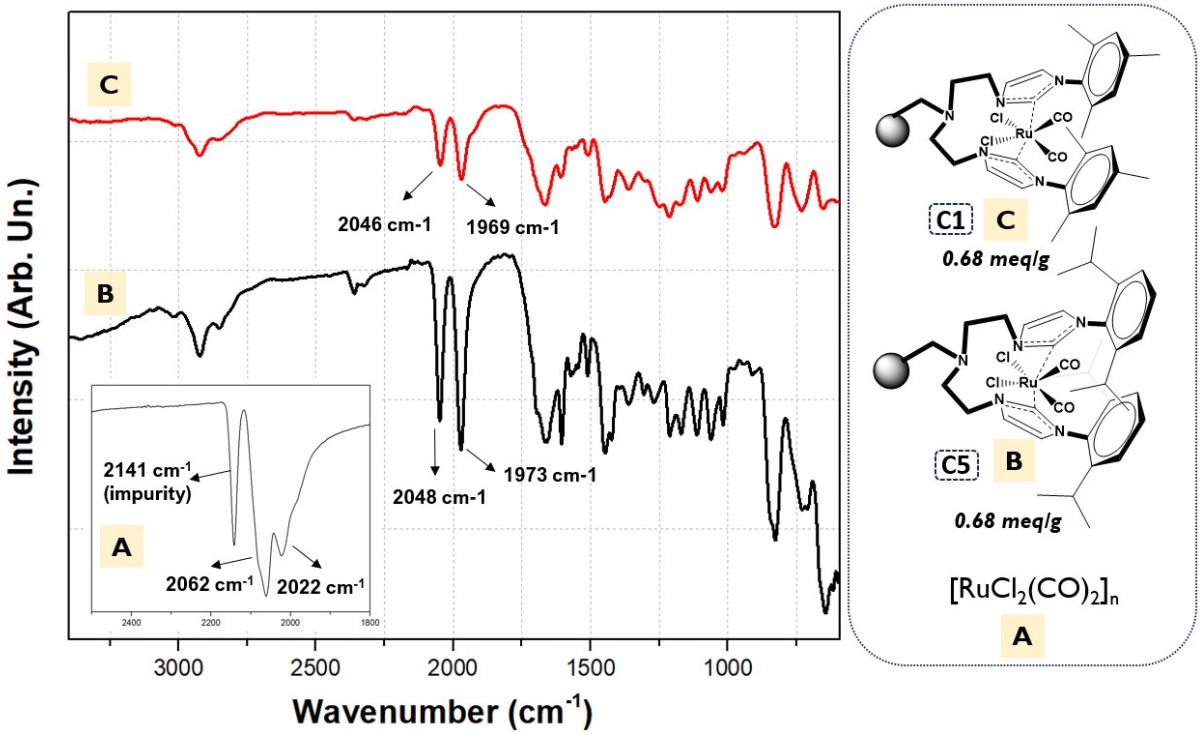

Figure S4. FTIR-ATR spectra of the $[RuCl_2(CO)_2]_n$ (A) and the supported Ru-NHC catalyst C5 (B) and C1 (C).

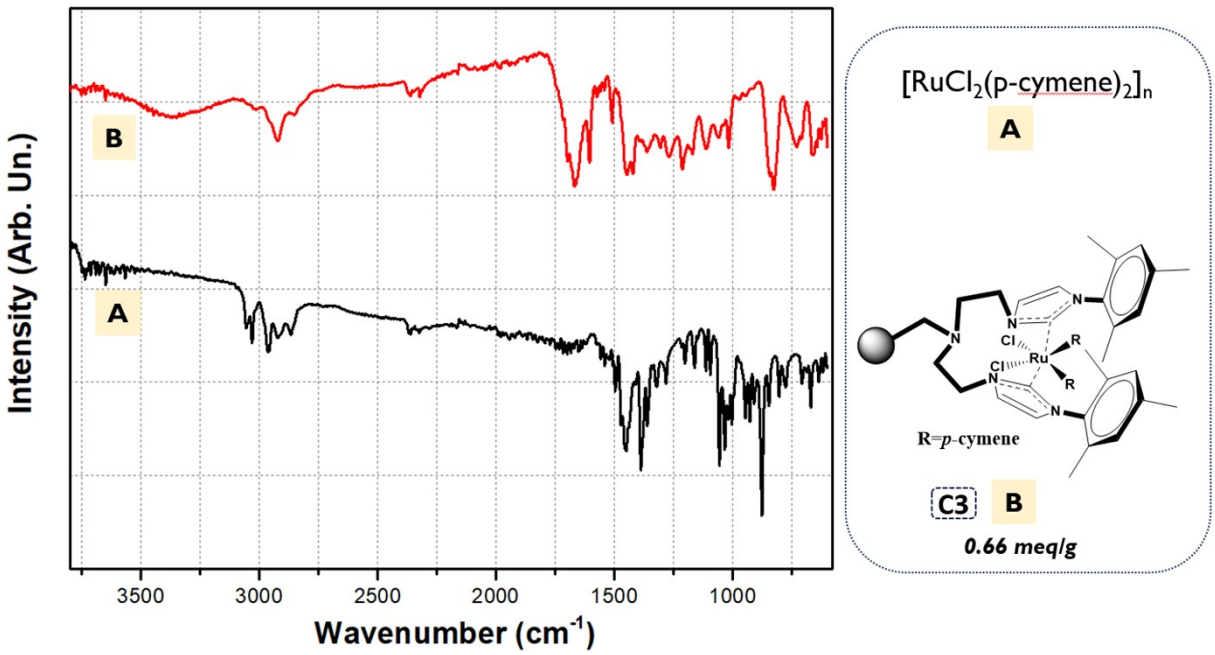

Figure S5. FTIR-ATR spectra of the $[RuCl_2$-(*p*-cymene$)_2]$ (A) and supported Ru-NHC catalyst C3 (B).

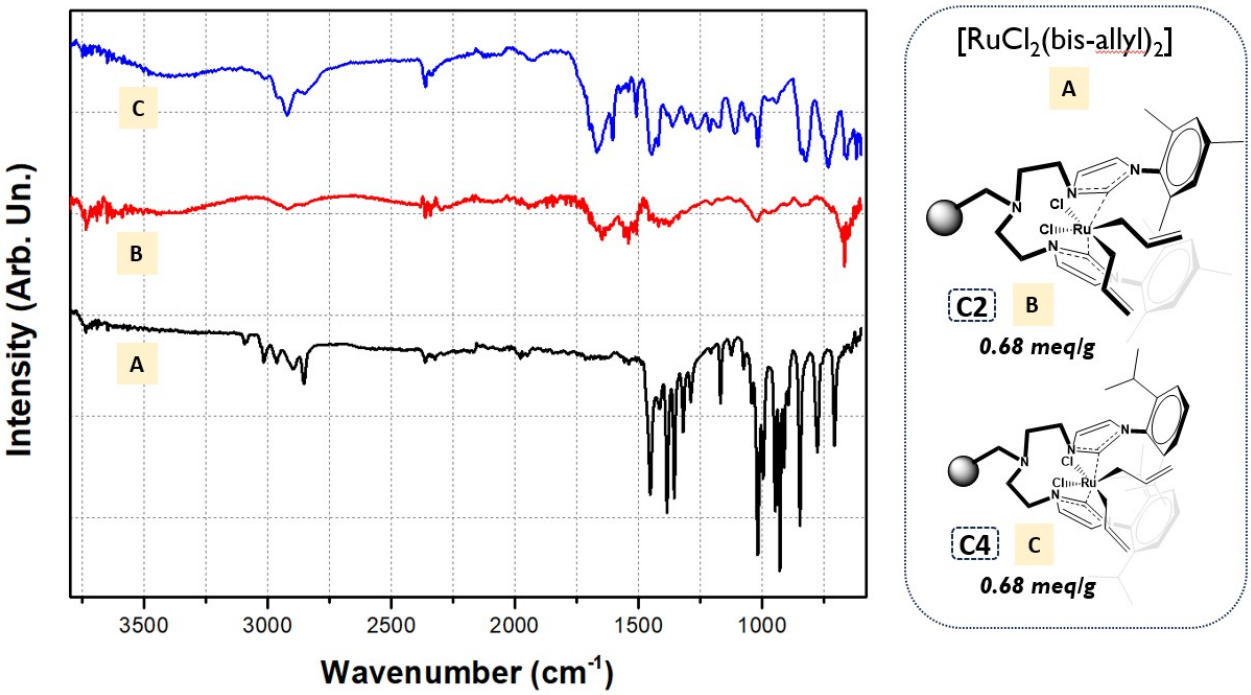

Figure S6. FTIR-ATR spectra of the $[RuCl_2(bis\text{-}allyl)_2]$ and related supported Ru-NHC catalysts C4 (B) and C2 (A).

S3.3. Ligand and Ru loading for each Ru-NHC-supported catalyst.

The quantification of Ru loading in the Ru-NHC-supported materials was performed by subjecting all the catalysts to acidic digestion using aqua regia. After the digestion process, the solutions were analyzed using ICP-MS to accurately obtain the Ru loading as mmol of Ru / g of support. In addition to measuring the Ru content, the loading of the NHC ligand on the Ru complexes was also determined through elemental analysis. By combining the results, a ratio pincer ligand Ru can be calculated for the different prepared Ru-NHC-supported catalysts. The results for each catalyst are detailed in Table S1.

Table S1. Metal and ligand loading for the supported Ru-NHC catalysts.

Catalyst	Ru loading [a] (mmol/g)	Ligand loading [b] (mmol/g)	Pincer-to-metal ratio [c]	Pincer free ligand(%) [d]	Pincer free ligand (%) determined by XPS
C1	0.168	0.68	8.1	43	40
C2	0.510	0.68	2.7	20	-
C3	0.296	0.66	4.5	36	42
C4	0.450	0.68	3.0	26	-
C5	0.167	0.68	8.1	43	-

a: Loading determined by ICP-MS after acidic digestion

b: Ligand loading obtained by nitrogen content determined by elemental analysis.

c: Pincer-to-metal ratio determined using the following equation: imidazolium loading (mmol/g) / Ru loading (mmol/g) m, where the imidazolium loading = ligand loading x 2.

d: Determined by using both the EA and ICP-MS analyses.

e: calculated using the ratio of the N1s of the deconvoluted bands of the XPs at ~399.6 eV for the carbene and the peak at ~402.3 eV related free imidazolium.

S3.3. XPS spectra of selected Ru-NHC-supported systems.

XPS spectra were obtained to investigate the electronic behaviour surrounding the Ru-NHC-supported systems. The XPS spectra for the Ru-NHC-supported C1, both before and after reuse, are shown in Figures S7 and S9. Additionally, the XPS spectra of the Ru-NHC-supported C3, which was prepared using $[RuCl_2(\text{bis-allyl})_2]$ instead of $[RuCl_2(CO)_2]_n$, are displayed in Figure S9.

Ru 3d XPS high-resolution spectra before (Figure S7) and after the reaction (Figure S9). Both spectra show a strong overlap between the C 1s and Ru 3d peaks. It is possible to identify the Ru $3d_5/_2$, while its corresponding spin-orbit splitting Ru $3d_3/_2$ is the one strongly overlapped with C 1s. To fit the spectra, eight components were used for the C1 as-prepared sample (Figure S7) and five components for C1 after its use in the reaction. For the C 1s corresponding to C1 as-prepared (Figure S7), the most intense C signal (blue) at 284.8 eV corresponds to C-(C,H) and/or adventitious carbon.[7] The olive, orange and purple peaks at 286.2, 287.4 and 289.0 eV were assigned to C-N, C-O and COOH, respectively.[7] Additionally, two extra components (violet) assigned to K+ species, correspond to the K 2p

spin-orbit splitting, K2$p_{3/2}$ and K 2$p_{1/2}$ centered at 293.5 / 296.3 eV, which can be related to remaining traces of KOtBu. All these components are accompanied by two additional ones related to Ru spin-orbit splitting, corresponding to one chemical species. The red doublet, located at 282.1 eV and 286.3 eV, was associated with the interaction between Ru and Cl (Ru-Cl) bonds.[8] Ru 3p analysis further supported this observation, identifying only Ru-Cl bonds, which is consistent with the structure of the Ru-NHC complex for C1. The presence of Cl was also evidenced in the Cl 2p high-resolution spectrum, where its spin-orbit splitting into Cl 2$p_3/_2$ and Cl 2$p_1/_2$ was peak-fitted using four components corresponding to two different chemical species. The first doublet (red), appearing at 198.3 eV and 199.9 eV, was associated with the interaction between Cl and Ru (Ru-Cl) bonds.[9, 10] The second doublet (purple), at 200.4 eV and 202.0 eV, corresponded to organic Cl as the counter ion of imidazolium.[10]

For the catalyst C1 after the reaction, the carbon species remain unchanged. However, the Ru doublet exhibited a shift towards lower binding energy, with peaks centered at 281.2 eV and 285.4 eV, suggesting a change in its chemical environment, indicating an interaction between Ru and O (Ru-O) bonds.[10] Additionally, the presence of two peaks centered at 462.5 eV and 485 eV, related to Ru 3$p_3/_2$ and Ru 3$p_1/_2$, respectively, clearly suggests the formation of RuO_2 nanoparticles after the reaction.

Noteworthy for both catalyst C1 and C3, the N1s spectra showed two different chemical environments, the olive peak at ~399.6 eV that corresponds to the interaction of C and N (C-N) bonds coordinated to Ru[8] and the wine peak at ~402.3 eV related to the presence of imidazolium (Figure S7 and S8).[10] Furthermore, by analyzing their N 1s XPS areas after deconvolution, we can deduce that approximately 60% of the NHC ligand is coordinated to Ru, and 40% is protonated (see Table S1 and S2).

Both peaks at *ca.* 399.6 eV and 402.3 eV are also presented in the spectra of C1 after its use (Figure S9). To identify the nature of Ru-NHC before and after the reaction, we performed an analysis summarized in Table S2. Before the reaction, neither Ru-O (typical of RuOx nanoparticles) nor Ru^{4+} were detected. Additionally, C-N, C-N imidazolium, and C-N carbene bonds were all present. A significant portion of the C-N signal originating from the tertiary amine connector was also observed in the bulk carbene complex. Interestingly, after the reaction, Ru-Cl and Ru^{3+} were no longer observed. Instead, we saw an increase in Ru-O bonds, characteristic of RuO_2 nanoparticles. The presence of these RuO_2 nanoparticles is primarily due to the isolation process of the supported systems, which is

carried out in air. Under the reaction conditions, with a large excess of hydrogen under pressure, it is likely that most of the RuO_2 is transformed into Ru(0), which is the active species in hydrogenation reactions. The C-N imidazole signal increased, while the C-N signal remained relatively unchanged. These findings support our hypothesis that some of the carbene transforms to stabilize the RuO_2 nanoparticles, while another portion remains associated with the free imidazole, whose signal intensifies after the reaction. The slight rise in C-N carbene along with the decrease in Ru-Cl might also indicate the breakdown of the Ru carbene complex and the further formation of RuO_2 nanoparticles.

Finally, the O 1s XPS high-resolution spectra before and after the reaction were fitted in both cases with two components. Before the reaction, two chemical species corresponding to C-O and COOH bonds were observed at 532.0 eV and 533.9 eV, respectively.[8, 10] After the reaction, the spectra also revealed two chemical species: one related to Ru-O bonds at 529.9 eV[11] and the other to C-O bonds at 532.4 eV.[10]

Table S2. Quantitative analysis (atomic %) obtained by XPS for the most relevant bonds.

Catalyst	Ru-O 281.2 ev	Ru-Cl 282.1 eV	$C\text{-}N_{(imidazolium)}$ 402.3 eV	$C\text{-}N_{(carbene)}$ 399.6 eV
C1-fresh	0	3.5*	2,59	1,73
C1-after 1st use	0,5**	0	3,93	1,78

*Corresponding to Ru^{3+} **Corresponding to Ru^{4+}. The analysis of C1 was performed after its first use.

Our most active catalyst, C1, was compared to the one with the lowest activity, C3 (using p-cymene), through XPS analysis (Figure S8). The Ru 3d spectrum confirms the presence of Ruthenium in the +3-oxidation state, likely in an octahedral geometry, as expected for this type of material. Additionally, it reveals the typical Ru-Cl bond. The N 1s spectrum shows a mix of imidazole and carbene functionalities in a ratio of 1.38:1. Finally, the Cl 2p spectrum again confirms the presence of Ru-Cl bonds at 198 eV.

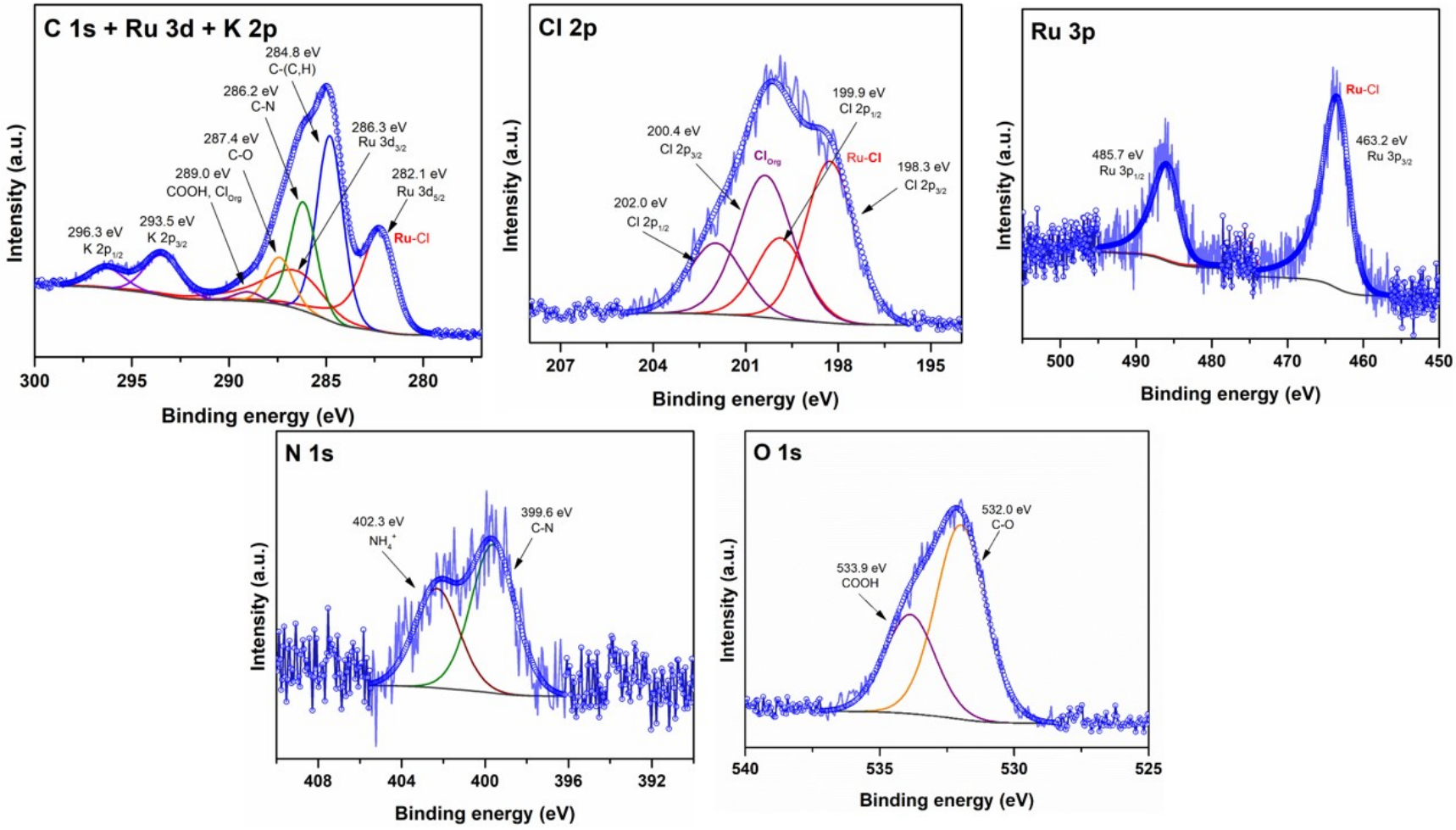

Figure S7. High-resolution XPS spectra for Ru-NHC-supported C1 as freshly prepared.

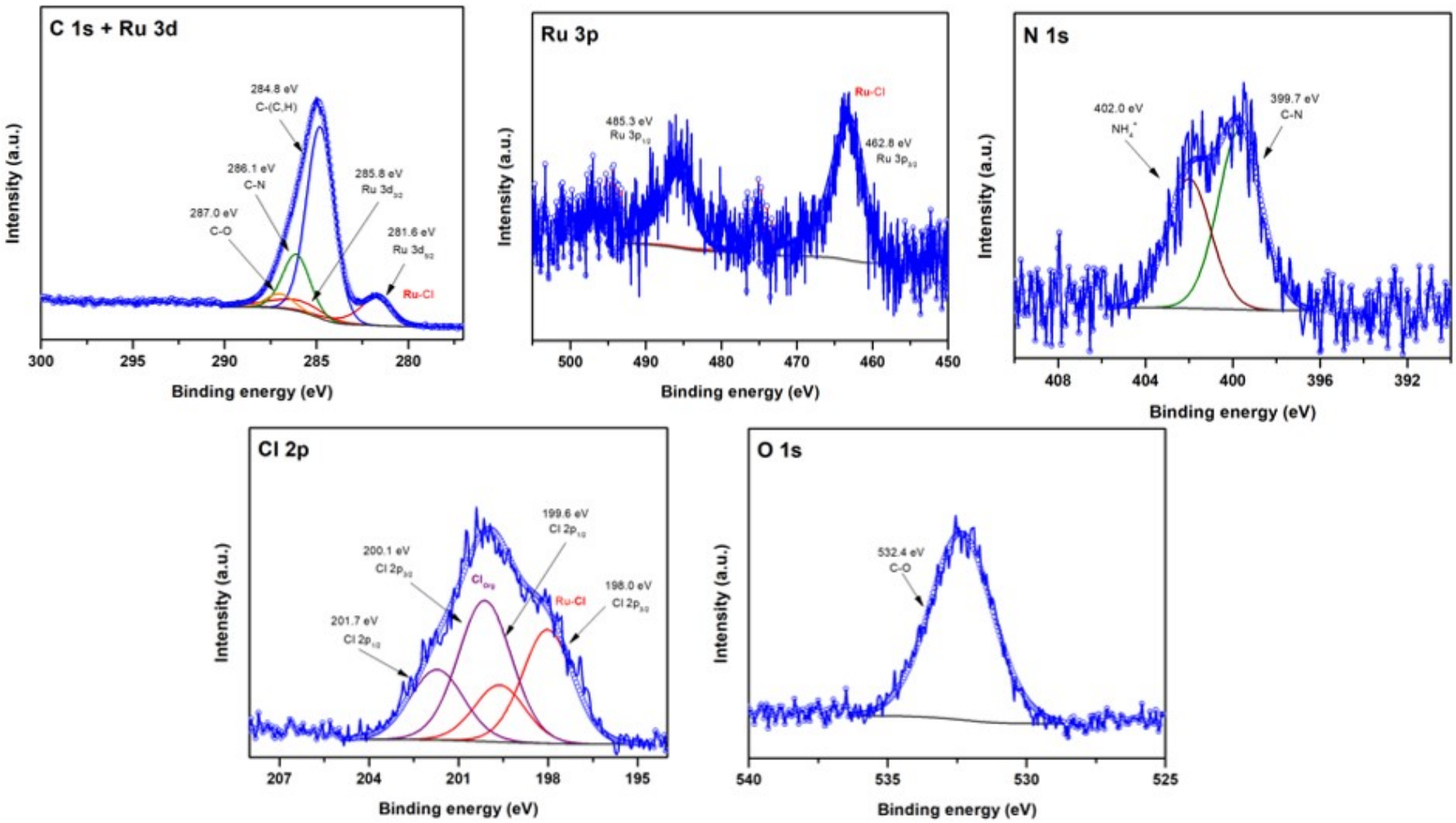

Figure S8. High-resolution XPS spectra for Ru-NHC-supported C3 as freshly prepared.

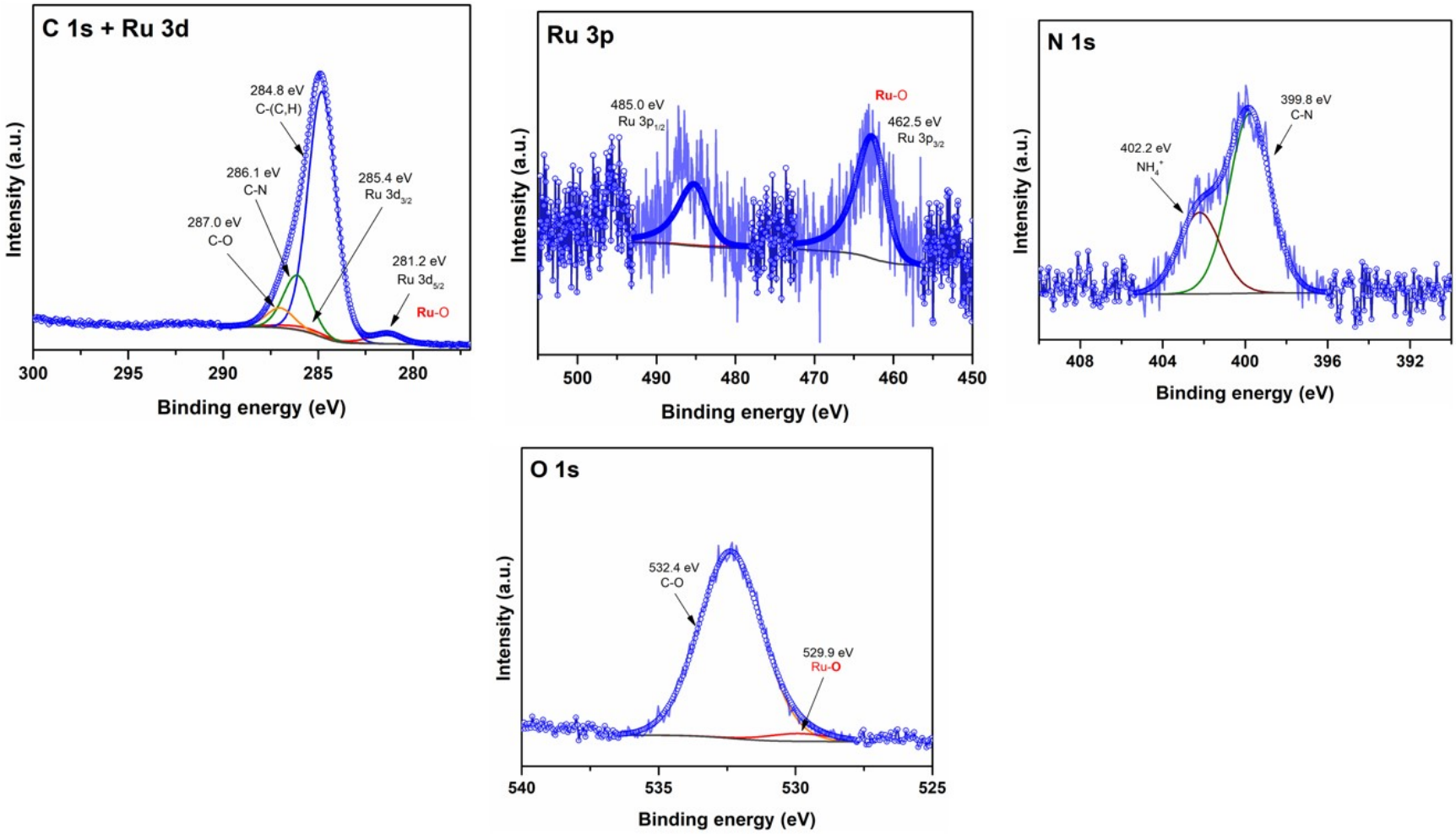

Figure S9. High-resolution XPS spectra for Ru-NHC-supported C1 after its use.

S4. TEM micrographs of the selected materials

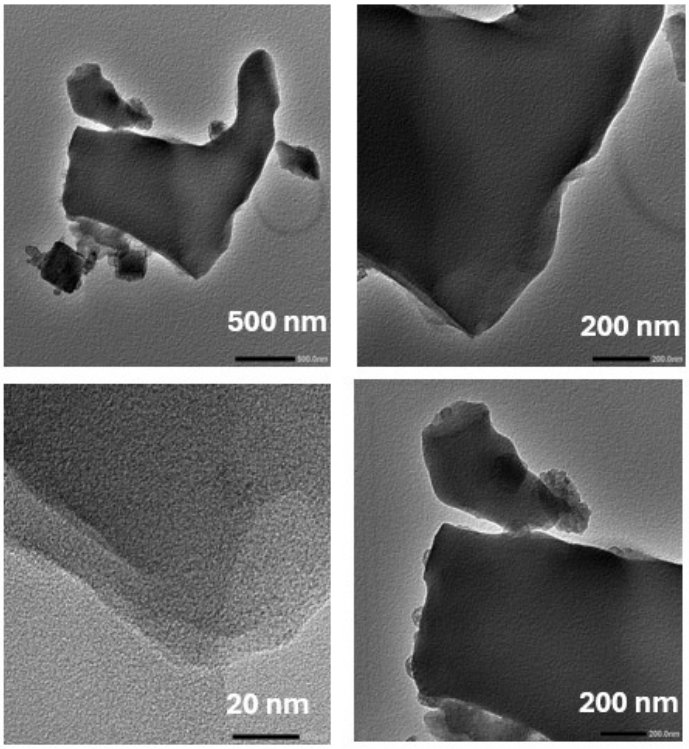

Figure S10. C1 before reaction

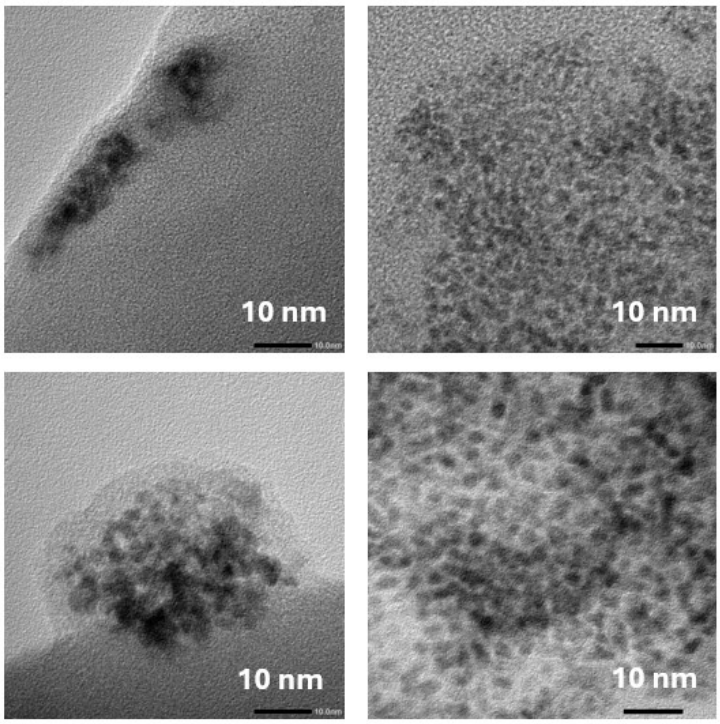

Figure S11. C1 after reaction

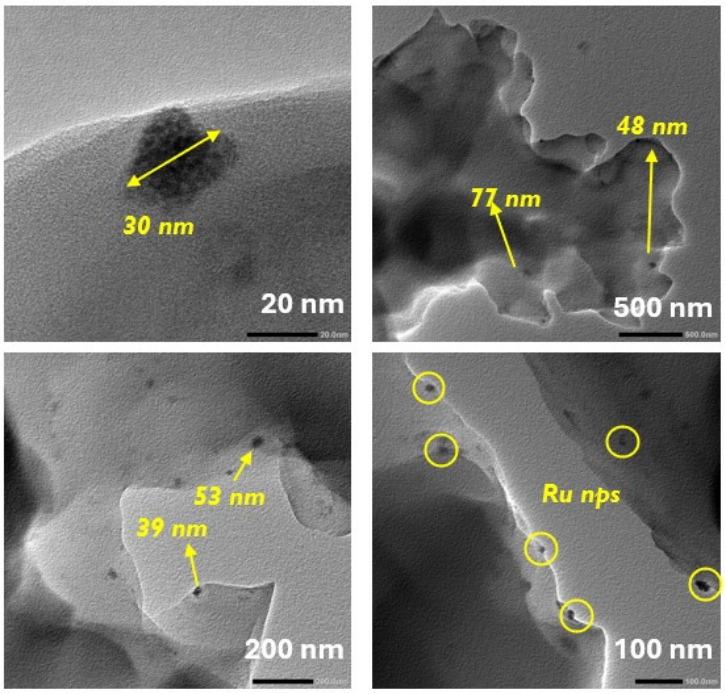

Figure S12. C3 after reaction

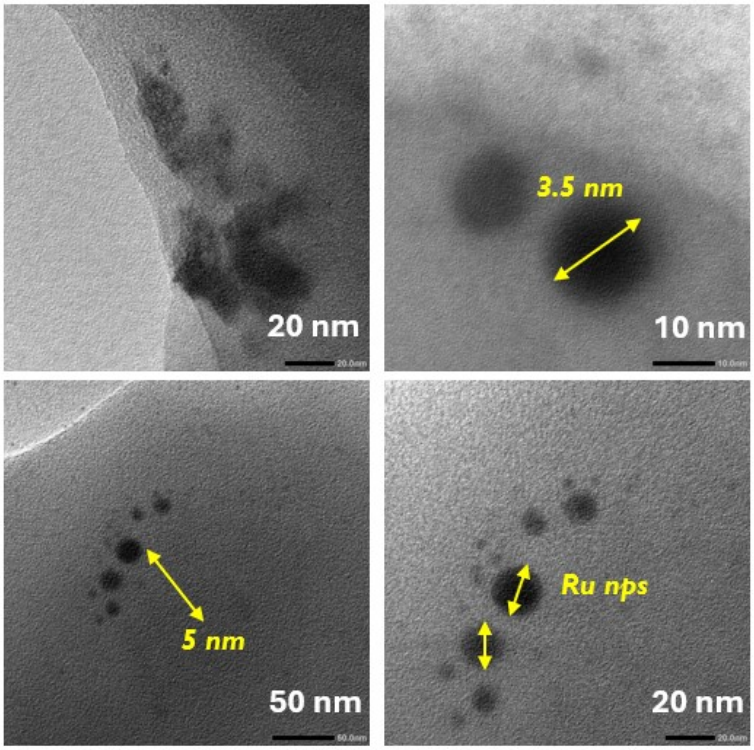

Figure S13. $[Ru(CO)_2Cl_2]_n$/4a

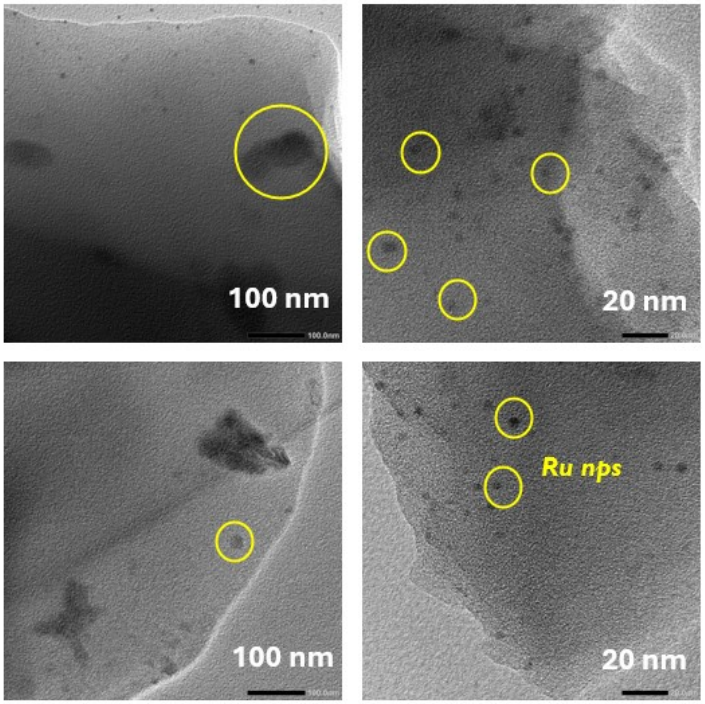

Figure S14. $RuCl_3$/4a (previously reduced before reaction)

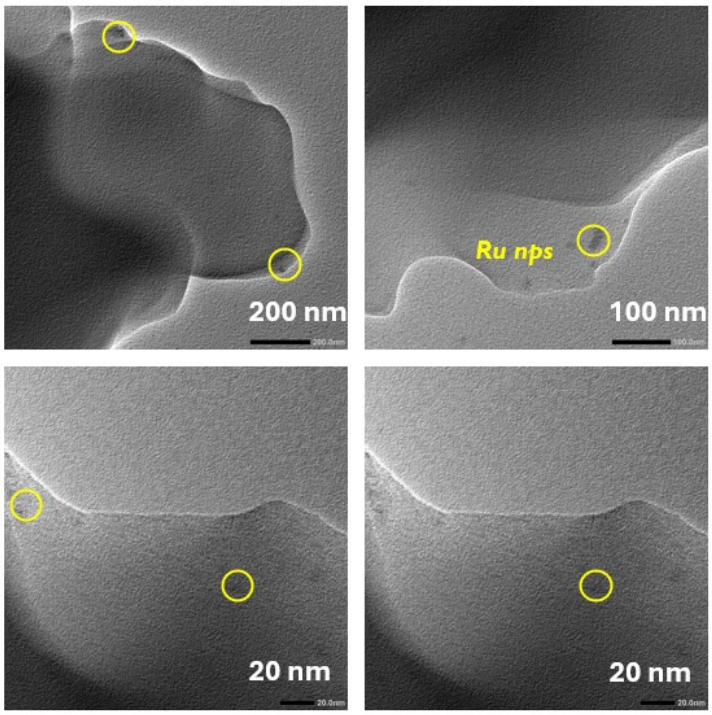

Figure S15. $RuCl_3$/4a (no reduced before reaction)

S5. Catalytic activity results of the $Ru(CO)_2Cl_2$/4a and $RuCl_3$/4a

To demonstrate that the supported Ru-NHC systems can serve both as chemical NHC–metal precursors for metal nanoparticles (MNPs) and as potential surface ligands for MNPs due to their strong affinity for forming robust bonds with metals, additional experiments were conducted. These experiments involved impregnating the same supported NHC-ligand and using either $[RuCl_2(CO)_2]_n$.or $RuCl_3$ as metal precursors. In this setup, the ligand behaves as a supported imidazolium system capable of adsorption and stabilization of the potential RuNPs particles formed directly without the assistance of the NHC ligand as a precursor (Figure S15).

In the first case, adsorbing $[RuCl_2(CO)_2]_n$ as a precursor resulted in significantly lower catalytic activity, reaching only 16%. Analysis of the catalyst after the reaction revealed the formation of small nanoparticles (15-20 nm, Figure S13), but no cluster formation was observed. Furthermore, less dispersed Ru nanoparticles were observed. Ru leaching was evident, as indicated by the presence of UV-Vis bands in the liquid phase after the reaction, which are assignable to Ru species (Figure S17). This finding underscores the vital role of pre-formed carbene species in stabilizing Ru nanoparticles. Although the nanoparticles formed during the reaction were small, they couldn't match the high yield achieved by C1 catalyst. This was true even when the reaction was conducted in the presence of TBAOAc and $TBA.HCO_3$, which can act as bases to facilitate the formation of RuNPs stabilized by NHC.

Two additional control tests were performed using $RuCl_3$ impregnated over supported imidazolium systems. In the first test, the catalyst was reduced before the reaction, while in the second, the catalyst was used as prepared. Under identical reaction conditions (temperature, pressure, and Ru metal amount), neither approach resulted in any catalytic activity. Interestingly, Ru nanoparticles were still observed (Figure S14 and S15), albeit smaller than those formed with the $[RuCl_2(CO)_2]_n$ system (4-10 nm, Figure S13). Consistent with the previous case, no cluster formation was detected, and the Ru nanoparticles weren't as highly dispersed as in our best catalyst.

The presence of well-defined and tuned Ru-NHC complexes is essential as a modifier to control both the NPs generation but also the activity and stability of these ligand-functionalized supported Ru NPs.

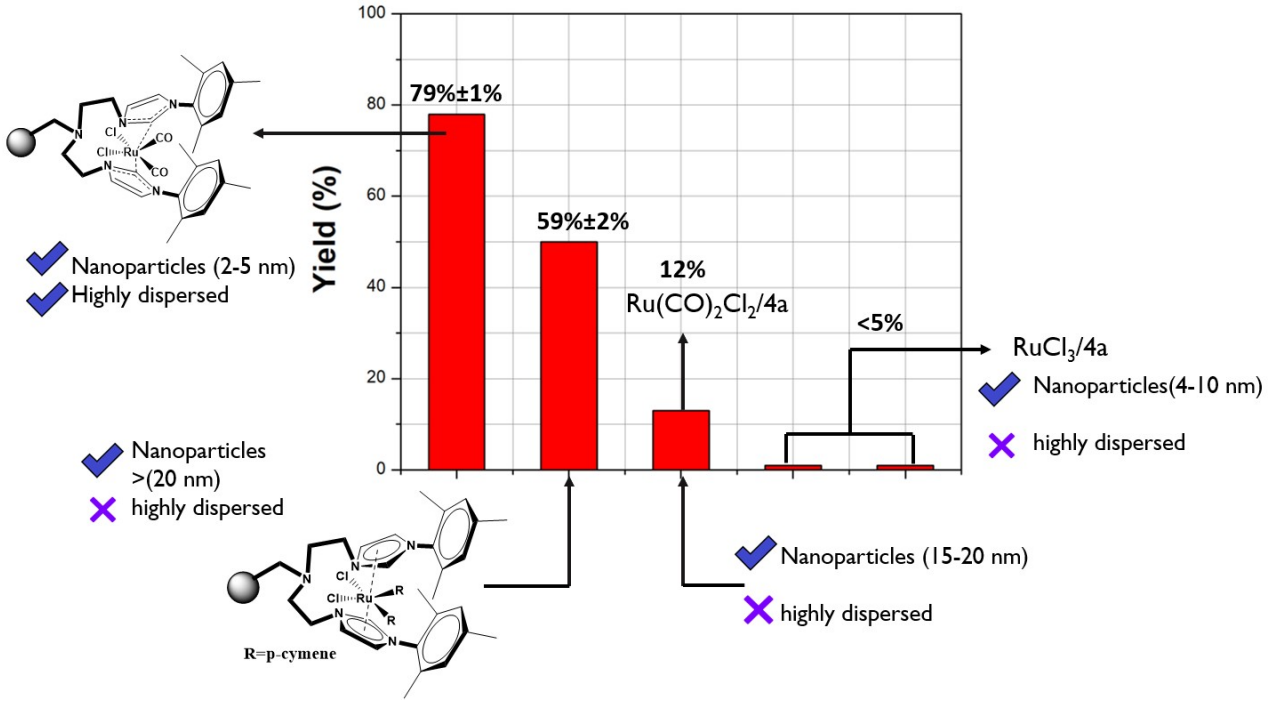

Figure S16. Comparison of the different catalytic activity for supported heterogeneous materials at the same reaction conditions (1 mmol TBA.HCO_3, 0.5 mmol TBA.OAc, 100°C, THF:water (1:1), 300 rpm, 30 bar H_2, 24 h.)

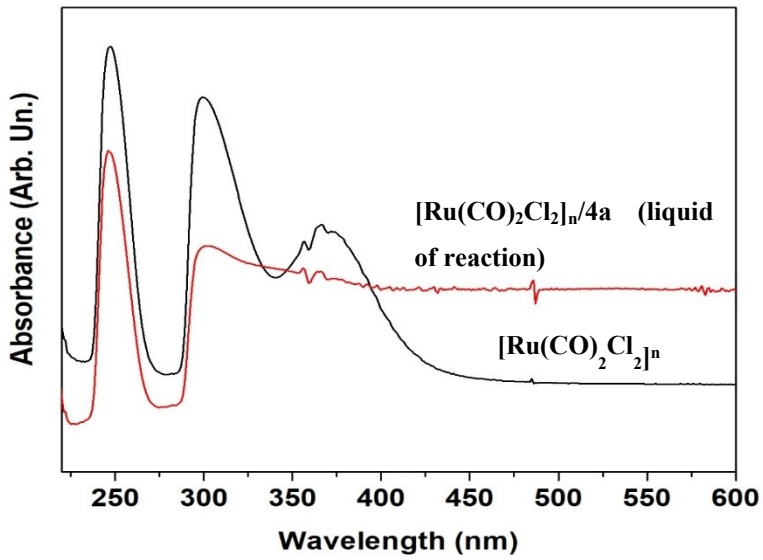

Figure S17. Comparison of the liquid of reaction using the $[Ru(CO)_2Cl_2]_n$/4a with the one homogeneous metallic precursor $[Ru(CO)_2Cl_2]_n$

S6. NMR data

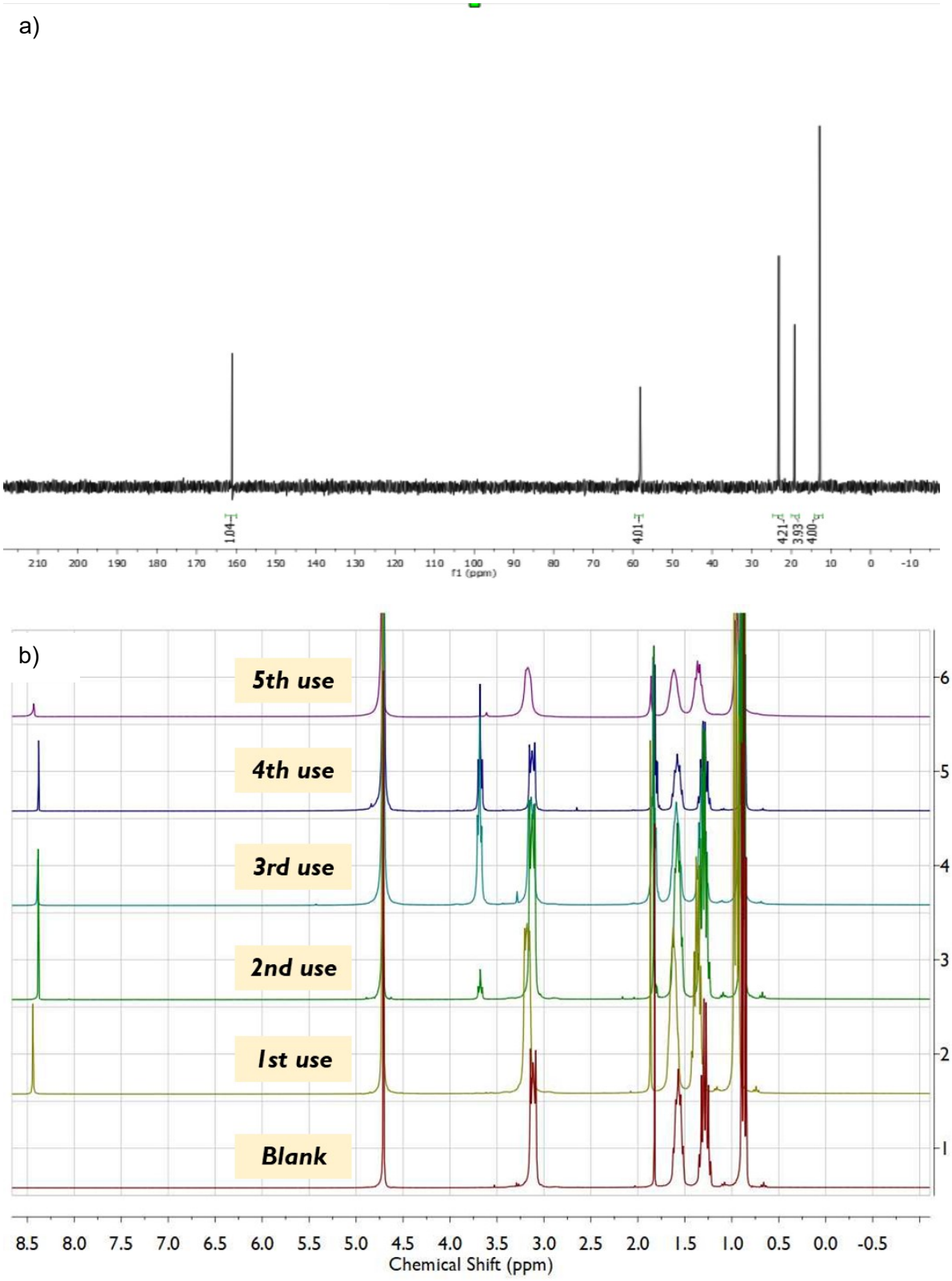

Figure S18. ^{13}C and ^{1}H NMR analysis of recycle test of hydrogenation reaction.

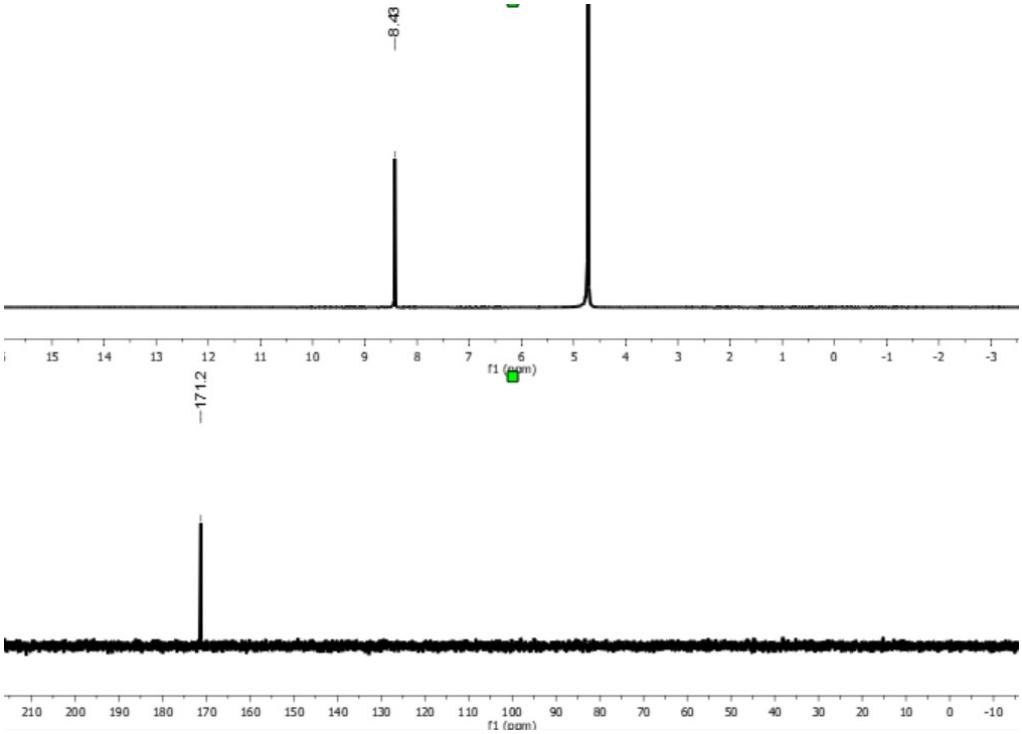

Figure S19. ^{1}H and ^{13}C NMR analysis of $NaHCO_2$ after cation exchange

S7. Determining Growth Rates in *C. necator* H16

C. necator H16 was cultivated in three independent 1 L-batch fermentations to establish its μ_{max} on 80 mM formic acid.

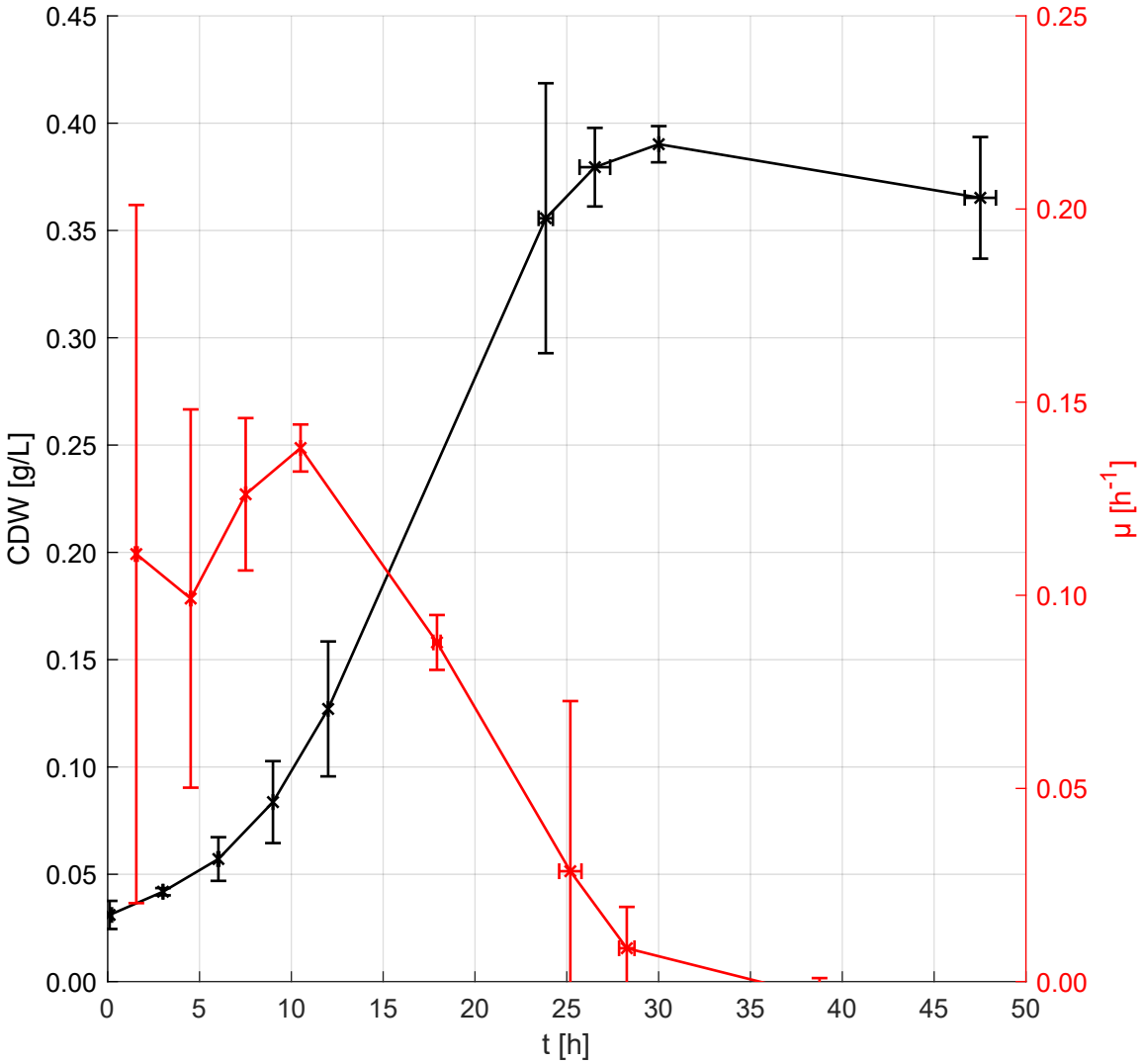

Figure S20. Biomass and growth rate profile of *C. necator* H16 in batch fermentation

S8. Adaptive Laboratory Evolution

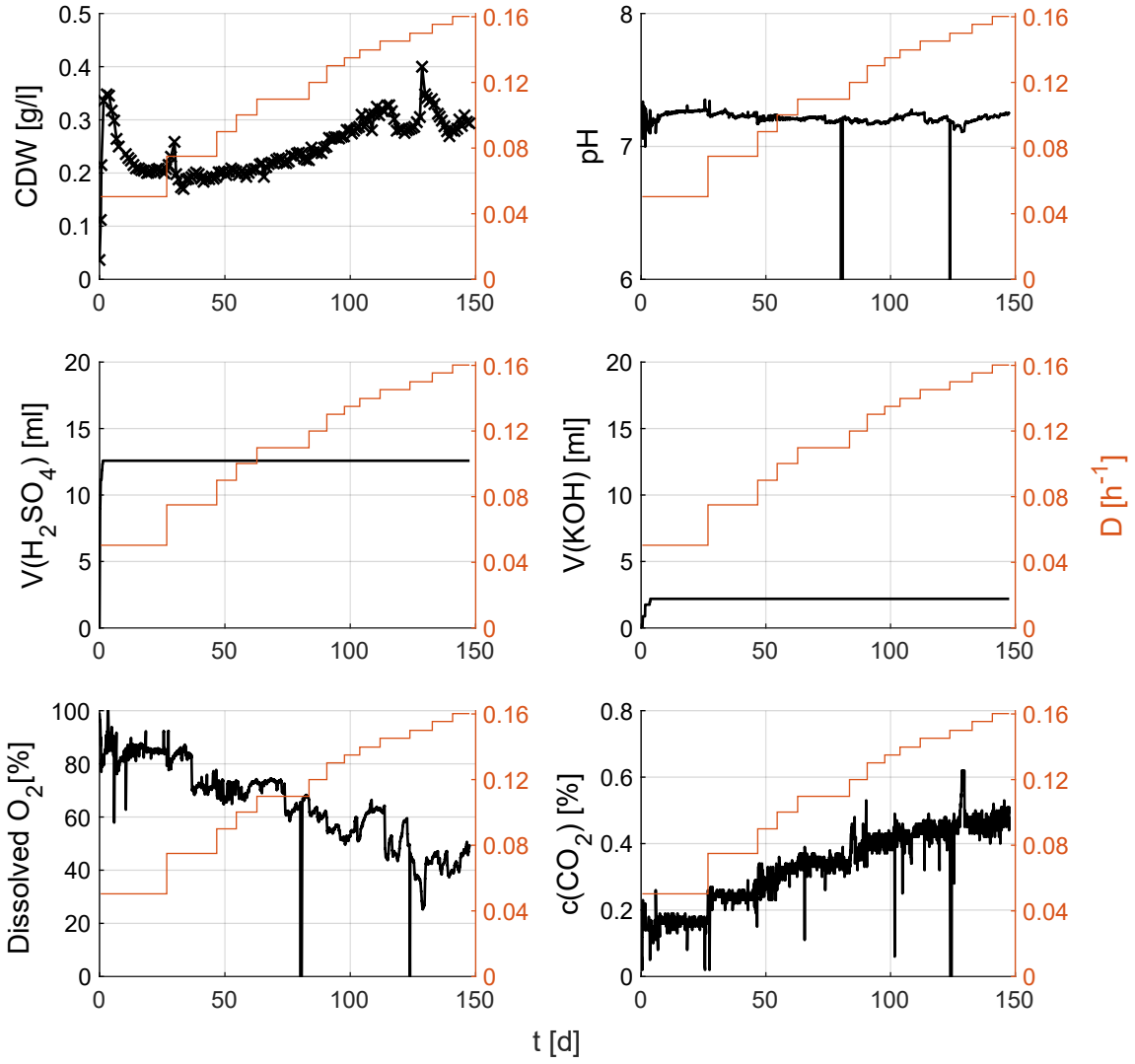

Figure S21. Biomass and online fermentation parameters during the Adaptive Laboratory Evolution (ALE) campaign.

For the evolution campaign, *C. necator* H16 was cultivated in a 1 L chemostat culture for 148 days. Samples were taken daily for offline biomass determination (CDW, top left). pH (top right), added volumes of acid and base (centre), dissolved oxygen (bottom left) and off-gas CO_2 concentrations (bottom right) were measured online through the ROSITA software. The dilution rate (D [h^{-1}], red, secondary Y-axis) was kept constant for at least five retention times before any further dilution rate increase.

S9.1 Screening of Evolved Strains

After initial small-scale screening of evolved strains in a BioLector, the best performing variants were carried forward to be tested for their growth rates in flasks. Strains *C. necator* ALE14, ALE25, ALE26 and ALE31 were grown in triplicates in 50 ml baffled flask cultures, along with a triplicate of the WT strain *C. necator* H16 on 80 mM formic acid.

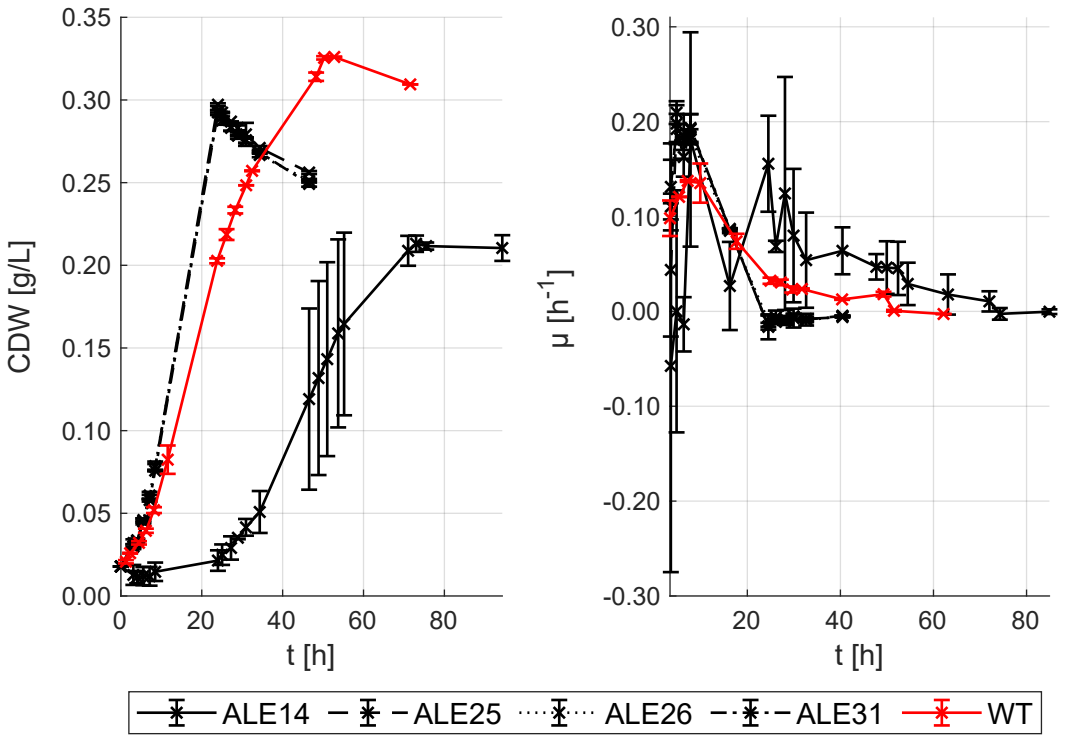

Figure S22. Biomass and growth rate profile of *C. necator* H16 and selected ALE variants

The resulting average CDW with standard deviations for error bars is shown on the left and growth rates, as calculated via a sliding window algorithm between two sampling points, shown on the right.

S9. Genetic Effects of the ALE Campaign

For an unbiased comparison, the genome of *C. necator* H16 as well as of the adapted strain ALE26 were sequenced with the INVIEW Resequencing of Bacteria service from Eurofins Scientific (Luxembourg, Luxembourg) (GenBank accession numbers: CP129213, CP129214). The average mean coverage for chromosome 1 and 2 in both cases was around 492 ± 74 sequences. However, while the coverage for pHG1 in the WT strain was 462.6 ± 60.1 sequences, in the evolved strain it was 0.8 ± 10.4. The sequence alignment showed that all sequences that were matched to the megaplasmid in *C. necator* ALE26 are located in regions where duplicates of genes are found that are also present on the other chromosomes. Matching these sequences against just chromosome 1 and 2 showed that they also fully align with the respective gene counterparts on these chromosomes. Therefore, the presence of the pHG1 megaplasmid could not be detected in the evolved strain.

To verify the plasmid's absence, polymerase chain reactions (PCRs) were performed, amplifying a region containing the RepB family plasmid replication initiator protein coding sequence (CDS) (see S2. Methods) by using both isolated plasmid as well as whole cells as template for the reaction. In both cases a clear band was evident for the WT strain in agarose gel electrophoresis at the expected size (Figure S23). However, that same band was absent for *C. necator* ALE26. The amplified region contains a repB family plasmid replication initiator protein CDS as well as part of the parA family protein CDS, both of which are surmised to be involved in plasmid maintenance upon cell division [12].

S10.1 Polymorphism Analysis of the genome of C. necator *ALE26*

All reads obtained via Illumina sequencing by Eurofins Genomics Limited (Ebersberg, Germany) were aligned against the published genome of *C. necator* H16 by Little et al. [2]. The consensus sequence of the reads was calculated with a 75 % threshold, calling a deletion for regions with no coverage and N if coverage was lower than 2 reads. The resulting polymorphisms for chromosome 1 and 2 are detailed in **Table S3** and **Table S4.**

Table S3*: Polymorphisms between chromosome 1 of* C. necator *H16 and* C. necator *ALE26 compared to the reference sequence*

Name	Minimum Position	Maximum Position	Change	Coverage	Polymorphism Type	Variant Frequency	Variant P-Value (approximate)	Amino Acid Change	CDS / gene
T	154,665	154,664	+T	348	Insertion	98.60%	0		

Name	Minimum Position	Maximum Position	Change	Coverage	Polymorphism Type	Variant Frequency	Variant P-Value (approximate)	Amino Acid Change	CDS / gene
T	333,427	333,427	G -> T	144	SNP (transversion)	99.30%	0		
C	384,989	384,989	G -> C	92	SNP (transversion)	25.00%	1.3E-50	G -> R	rsmD CDS
G	627,928	627,928	C -> G	65	SNP (transversion)	40.00%	3.8E-58	A -> G	AEC family transporter CDS
A	627,936	627,936	C -> A	43	SNP (transversion)	76.70%	2.4E-100	P -> T	AEC family transporter CDS
A	791,503	791,503	C -> A	199	SNP (transversion)	96.50%	0	G -> W	YgcG family protein CDS
	913,393	913,393	-G	493	Deletion	100.00%	0		DUF1329 domain-containing protein CDS
GG	1,061,461	1,061,462	CT -> GG	55 -> 56	Substitution	26.8% -> 32.7%	7.2E-31	S -> P	PLP-dependent aminotransferase family protein CDS
T	1,104,731	1,104,731	G -> T	298	SNP (transversion)	98.00%	0		
A	1,190,158	1,190,158	C -> A	247	SNP (transversion)	95.50%	0	G -> W	hypothetical protein CDS
T	1,211,314	1,211,314	G -> T	160	SNP (transversion)	95.60%	0	G -> V	aldehyde dehydrogenase CDS
T	1,559,970	1,559,970	G -> T	115	SNP (transversion)	94.80%	0		
T	1,628,903	1,628,903	G -> T	353	SNP (transversion)	96.30%	0	R -> S	glucose-6-phosphate isomerase CDS
C	1,636,643	1,636,643	A -> C	75	SNP (transversion)	34.70%	3.8E-56		
TA	1,807,929	1,807,930	AT -> TA	513 -> 514	Substitution	99.40%	7.6E-201		23S rRNA
GCAC	1,807,933	1,807,936	TGTT -> GCAC	517 -> 524	Substitution	99.60%	1.2E-204		23S rRNA
CA	1,807,940	1,807,941	GG -> CA	521 -> 523	Substitution	99.00%	3.2E-201		23S rRNA
GG	1,807,947	1,807,946	(GG)2 -> (GG)3	517 -> 522	Insertion (tandem repeat)	100.00%	1.6E-207		23S rRNA
G	2,101,218	2,101,218	A -> G	88	SNP (transition)	25.00%	4.4E-44	W -> R	D-galactonate dehydratase family protein CDS

Name	Minimum Position	Maximum Position	Change	Coverage	Polymorphism Type	Variant Frequency	Variant P-Value (approximate)	Amino Acid Change	CDS / gene
T	2,108,292	2,108,292	G -> T	228	SNP (transversion)	100.00%	0	G -> V	hypothetical protein CDS
C	2,517,531	2,517,531	G -> C	74	SNP (transversion)	27.00%	5.5E-41		
A	2,597,067	2,597,067	C -> A	245	SNP (transversion)	99.60%	0	G -> V	adenosylcobalamin-dependent ribonucleoside-diphosphate reductase CDS
A	2,619,321	2,619,321	C -> A	260	SNP (transversion)	98.50%	0	G -> V	ABC transporter ATP-binding protein CDS
T	3,162,470	3,162,470	G -> T	83	SNP (transversion)	90.40%	3.9E-230	G -> V	TRAP transporter large permease subunit CDS
T	3,393,896	3,393,896	G -> T	240	SNP (transversion)	97.50%	0	P -> Q	glutamate-5-semialdehyde dehydrogenase CDS
C	3,575,406	3,575,405	(C)4 -> (C)5	625	Insertion (tandem repeat)	100.00%	3.2E-188		23S rRNA
C	3,780,743	3,780,742	(C)4 -> (C)5	63	Insertion (tandem repeat)	100.00%	1.3E-19		23S rRNA
A	3,811,856	3,811,856	C -> A	204	SNP (transversion)	99.00%	0		gspD CDS
A	3,811,867	3,811,867	C -> A	210	SNP (transversion)	99.50%	0	A -> D	gspD CDS

Table S4*: Polymorphisms between chromosome 2 of* C. necator *H16 and* C. necator *ALE26*

Name	Minimum	Maximum	Change	Coverage	Polymorphism Type	Variant Frequency	Variant P-Value (approximate)	Amino Acid Change	CDS
C	65,449	65,449	A -> C	96	SNP (transversion)	28.10%	5.0E-58		
G	177,508	177,507	(G)3 -> (G)4	642	Insertion (tandem repeat)	99.80%	1.6E-190		23S rRNA
G	178,375	178,374	(G)5 -> (G)6	615	Insertion (tandem repeat)	100.00%	3.2E-185		23S rRNA

Name	Minimum	Maximum	Change	Coverage	Polymorphism Type	Variant Frequency	Variant P-Value (approximate)	Amino Acid Change	CDS
G	649,715	649,715	C -> G	80	SNP (transversion)	25.00%	3.4E-44		hypothetical protein CDS
A	659,277	659,277	C -> A	100	SNP (transversion)	82.00%	1.2E-243	R -> S	sensor histidine kinase CDS
GGG	676,319	676,321	ATC -> GGG	57 -> 61	Substitution	25.9% -> 27.9%	2.0E-26		
G	676,326	676,326	T -> G	51	SNP (transversion)	27.50%	3.1E-29		
A	772,834	772,834	C -> A	148	SNP (transversion)	94.60%	0.0E+00	P -> T	HlyD family type I secretion periplasmic adaptor subunit CDS
G	870,539	870,538	(G)4 -> (G)5	545	Insertion (tandem repeat)	99.80%	1.7E-161		23S rRNA
C	871,061	871,060	(C)4 -> (C)5	133	Insertion (tandem repeat)	98.50%	1.3E-49		23S rRNA
G	1,400,099	1,400,099	C -> G	78	SNP (transversion)	34.60%	2.6E-66		
C	1,400,107	1,400,107	G -> C	84	SNP (transversion)	25.00%	2.0E-48		
C	1,400,109	1,400,109	G -> C	86	SNP (transversion)	29.10%	9.6E-67		
T	1,553,621	1,553,621	G -> T	96	SNP (transversion)	97.90%	2.9E-260	P -> T	gph CDS
C	1,622,546	1,622,546	T -> C	84	SNP (transition)	32.10%	7.1E-60		
A	1,911,223	1,911,223	C -> A	227	SNP (transversion)	96.90%	0.0E+00	R -> L	amino acid adenylation domain-containing protein CDS
G	2,363,459	2,363,459	T -> G	97	SNP (transversion)	28.90%	7.1E-69		
T	2,453,032	2,453,032	G -> T	219	SNP (transversion)	97.70%	0.0E+00		ferritin-like domain-containing protein CDS
C	2,637,816	2,637,816	G -> C	56	SNP (transversion)	25.00%	5.6E-30	R -> P	diguanylate cyclase CDS
CC	2,637,818	2,637,819	GA -> CC	63 -> 66	Substitution	33.3% -> 34.8%	2.7E-47	D -> P	diguanylate cyclase CDS

Several other polymorphisms have been observed on the two main chromosomes compared to the published reference sequence (Table S3 and Table S4). Notably, the majority of these can also be observed in the sequence of the WT strain used in this study. The only mutations

unique to *C. necator* ALE26 are listed in Table S5. Of these, only two are in regions coding for a gene. The gene affected on chromosome 1 (DUF1329 domain-containing protein CDS) is of unknown function and can therefore not be tied to any biochemical processes. The other gene, annotated as a diguanylate cyclase, is found in several *Cupriavidus* strains and is speculated to be involved in signal transduction.[52] Conserved domains are found in other bacterial species like *Pseudomonas*[53] but its function in *C. necator* H16 is unknown.

Table S5: Polymorphisms unique to C. necator *ALE26 across chromosomes 1 and 2*

Chromosome	**Minimum Position**	**Maximum Position**	**Change**	**Coverage**	**Coding sequence**	**Amino Acid effect**
Chromosome 1	913,393	913,393	-G	493	DUF1329 domain-containing protein	Frame shift
Chromosome 2	65,449	65,449	A -> C	96	none	none
Chromosome 2	676,326	676,326	T -> G	51	none	none
Chromosome 2	1,622,546	1,622,546	T -> C	84	none	none
Chromosome 2	2,637,818	2,637,819	GA -> CC	63 -> 66	diguanylate cyclase	D -> P

Both, the adapted as well as the WT strain used in this study harbour a point mutation in the glucose-6-phosphate isomerase gene (locus tag: E6A55_07580, R222S). For both strains growth on fructose resulted in long lag phases and reduced biomass compared to literature values and growth on similar substrates like sodium gluconate (data not shown).

S10.2 PCR of pHG1

Presence of the megaplasmid pHG1 in *C. necator* H16 and ALE26 was determined using PCR of both isolated plasmid and whole cells.

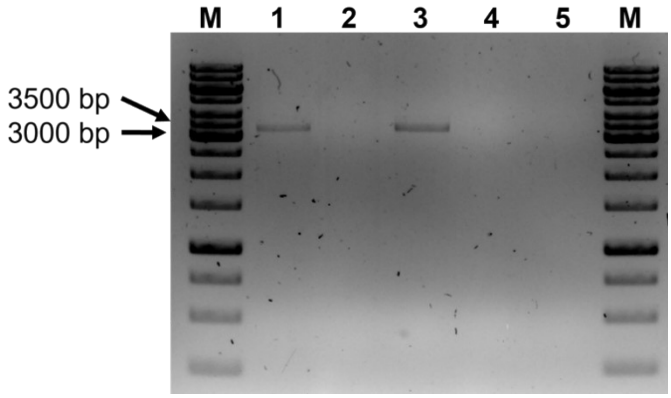

Figure S23. PCR results for checking the presence of pHG1 in *C. necator* H16 and ALE26

The presence of pHG1 in each strain was assed via PCR using primers pHG1_pF and pHG1_pR (expected product size: 3266 bp). For each strain, the plasmid was extracted using a Plasmid Midi Kit (Qiagen, Hilden, Germany). Additionally, colony PCRs were performed for each, using whole cells as the template for the reaction. The wells were loaded as follows: M: GeneRuler 1 kb DNA Ladder (Thermo Fisher Scientific, Waltham, MA, USA); 1: *C. necator* H16 pHG1 extraction; 2: *C. necator* ALE26 pHG1 extraction; 3: *C. necator* H16 colony PCR; 4: *C. necator* ALE26 colony PCR; 5: negative control, no template DNA.

S10. Functional Changes in the Evolved Strain

Proteomic Comparison of C. necator *H16 and ALE26*

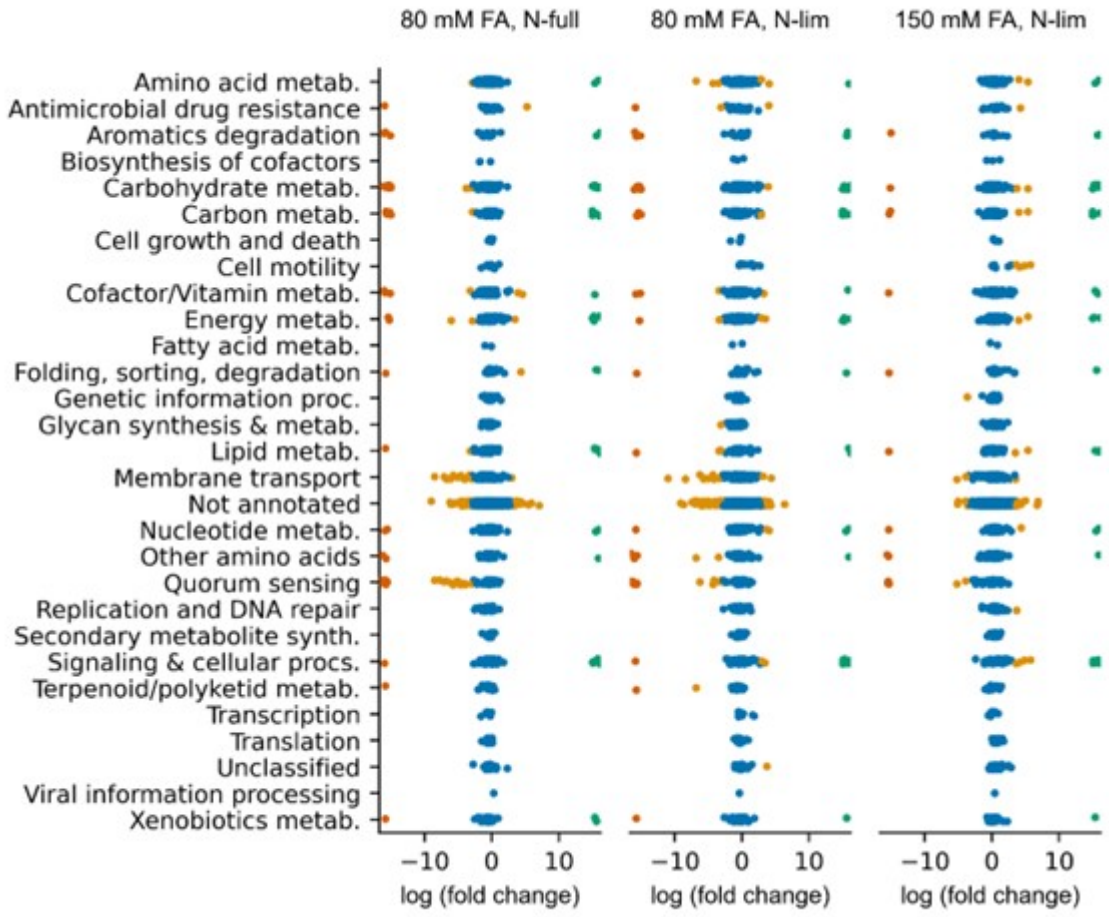

Figure S24. Influence of the ALE campaign of the *C. necator* proteome

The proteome of *C. necator* ALE26 was compared to that of the wildtype strain in continuous cultivation under nitrogen non-limiting (N-full) and limiting (N-lim) conditions with two different carbon concentrations used in the limited condition. More negative *log*(fold change) values indicate higher expression in the adapted strain while positive values suggest increased expression in *C. necator* H16. Each dot represents a single protein, with blue dots (●) showing no statistically significant change between conditions (adjusted $\alpha > 0.05$) and orange dots (●) representing those that are statistically significantly differentially expressed. Proteins shown in red (●) are only found in the adapted strain and those in green (●) only in the wildtype. As the fold change of comparing any number against 0 would be infinite, the *log*(fold change) values at which these are plotted are arbitrary and not the result of a statistical comparison.

S11. Growth Profiles of Continuous Fermentations to Produce PHB in *C. necator* ALE26

To assess PHB accumulation in *C. necator* ALE26 in continuous cultivation, several process parameters were investigated for optimisation. The C/N ratio was the first parameter whose influence on PHB production was investigated. To this end, a continuous fermentation at a constant dilution rate of 0.15 h^{-1} and 80 mM formic acid in the feed medium was run under varying nitrogen concentrations in the feed (Figure S25). The highest ratio tested (264.28 mol/mol) is equivalent to that used in batch shake flask experiments. However, in the chemostat the resulting biomass was too low to allow for harvesting without almost entirely draining the reactor. Thus, the highest C/N ratio tested for intracellular PHB was 150 mol/mol. Once the reactor had stabilised at that condition, samples for biological duplicates were taken before the C/N ratio was decreased by 25 mol/mol. This was repeated until a ratio of 25 mol/mol was reached. Ratios of 50 mol/mol and 150 mol/mol were then tested again to ensure that any observed trend in the PHB content would not be the result of a systematic error arising from the order in which the conditions were tested.

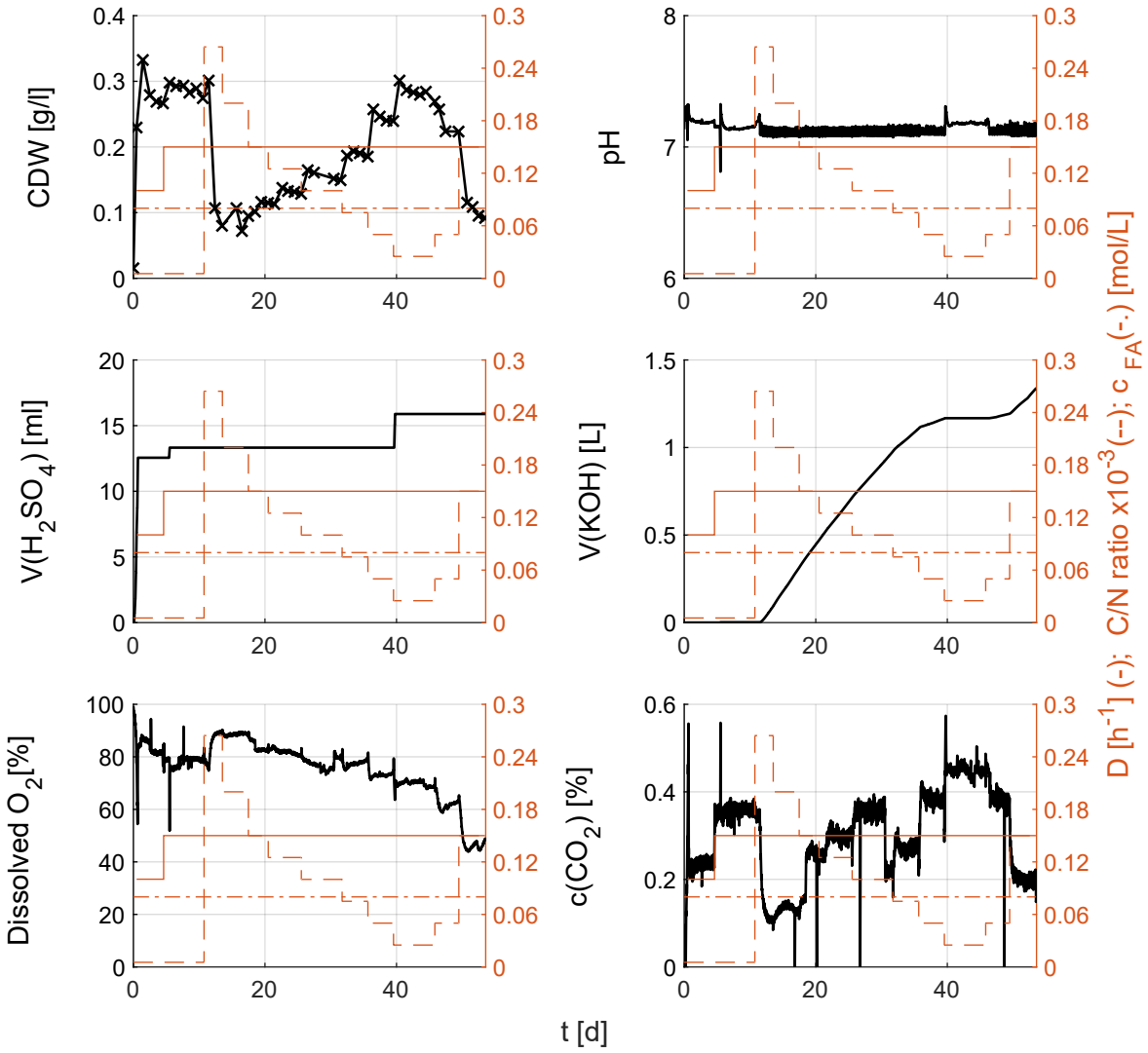

Figure S25. Biomass and online fermentation parameters during varying C/N ratios for PHB production

To test PHB production in *C. necator* ALE26 in varying C/N ratios ([mol/mol], --, dashed red line, secondary Y-axis), the organism was cultivated in a 1 L chemostat culture. Samples were taken daily for offline biomass determination (CDW, top left). pH (top right), added volumes of acid and base (centre), dissolved oxygen (bottom left) and off-gas CO_2 concentrations (bottom right) were measured online through the ROSITA software. The dilution rate (D [h^{-1}], -, full red line, secondary Y-axis) was kept constant at 0.15 h^{-1} for the entire nitrogen-limited phase of the experiment, while the formic acid concentration in the feed remained at 80 mM (-.,dash-dotted red line, secondary Y-axis).

In a second fermentation, varying dilution rates were applied and PHB production was again monitored. Based on the results from the first fermentation, the formic acid concentration

was kept at 80 mM in the feed and the C/N ratio at 50 mol/mo. Dilution rates were tested between 0.050 h^{-1} and 0.165 h^{-1} (Figure S26).

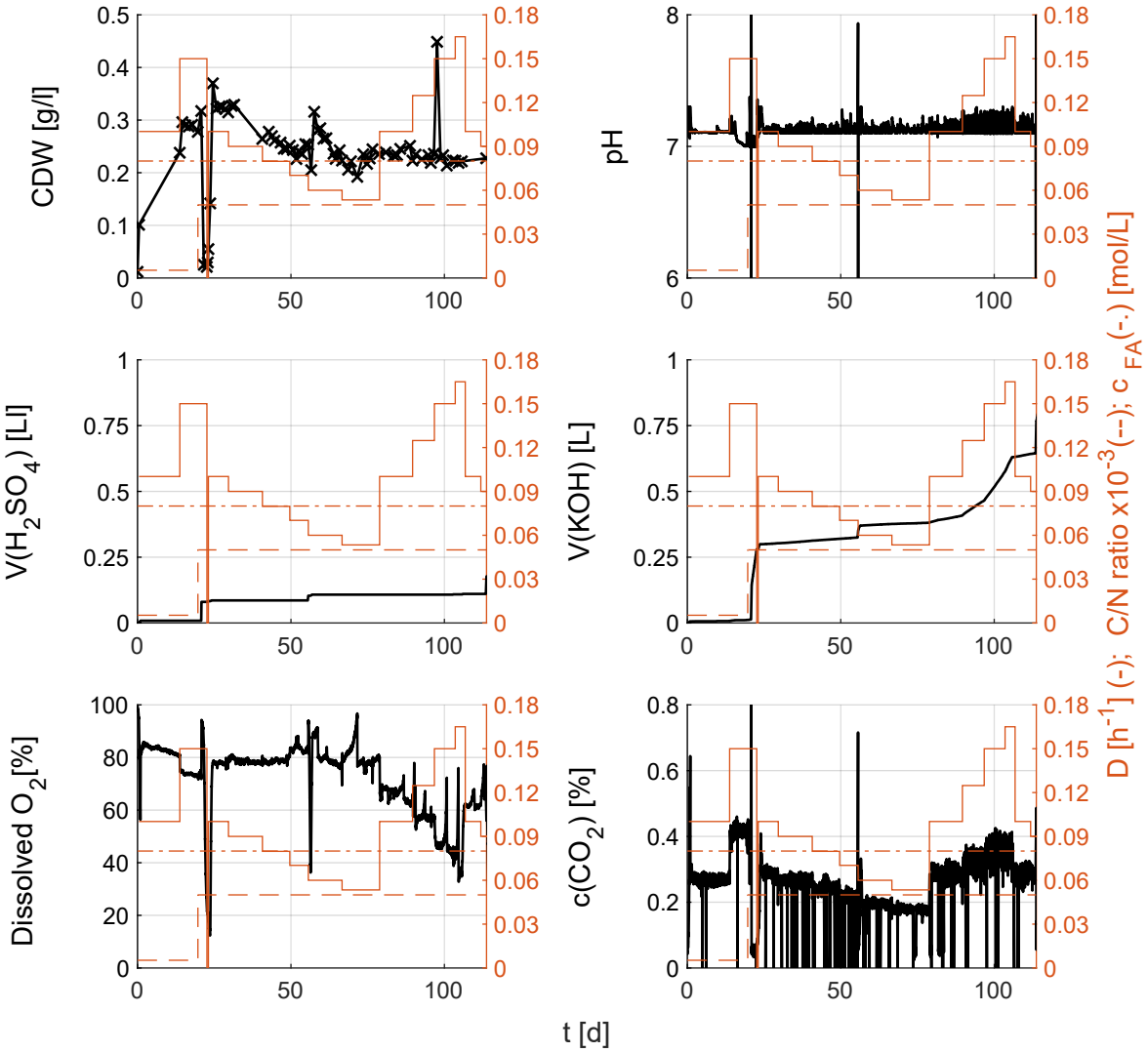

Figure S26. Biomass and online fermentation parameters during varying diltuion rates for PHB production

To test PHB production in *C. necator* ALE26 in varying dilution rates (D [h^{-1}], -, full red line, secondary Y-axis), the organism was cultivated in a 1 L chemostat culture. Samples were taken daily for offline biomass determination (CDW, top left). pH (top right), added volumes of acid and base (centre), dissolved oxygen (bottom left) and off-gas CO_2 concentrations (bottom right) were measured online through the ROSITA software. The C/N ratio (--, dashed red line, secondary Y-axis) was kept constant at 50 mol/mol for the entire nitrogen-limited phase of the experiment, while the formic acid concentration in the feed remained at 80 mM (-., dash-dotted red line, secondary Y-axis).

Finally, the formic acid concentration was increased stepwise in a third continuous fermentation while keeping the C/N ratio at 50 mol/mol and the dilution rate at 0.09 h^{-1}. The biomass as determined by OD_{600} measurements increased with each increase of the supplied carbon source (Figure S27). Due to the accumulation of formic acid in the fermenter in the growth-limited condition, a continuous addition of KOH to the vessel was observed to keep the pH stable. The change in rate of base addition followed the trend of the supplied amount of formic acid. The dissolved oxygen decreased with an increase in biomass whilst the CO_2 concentration in the off-gas increased indicating more active biomass.

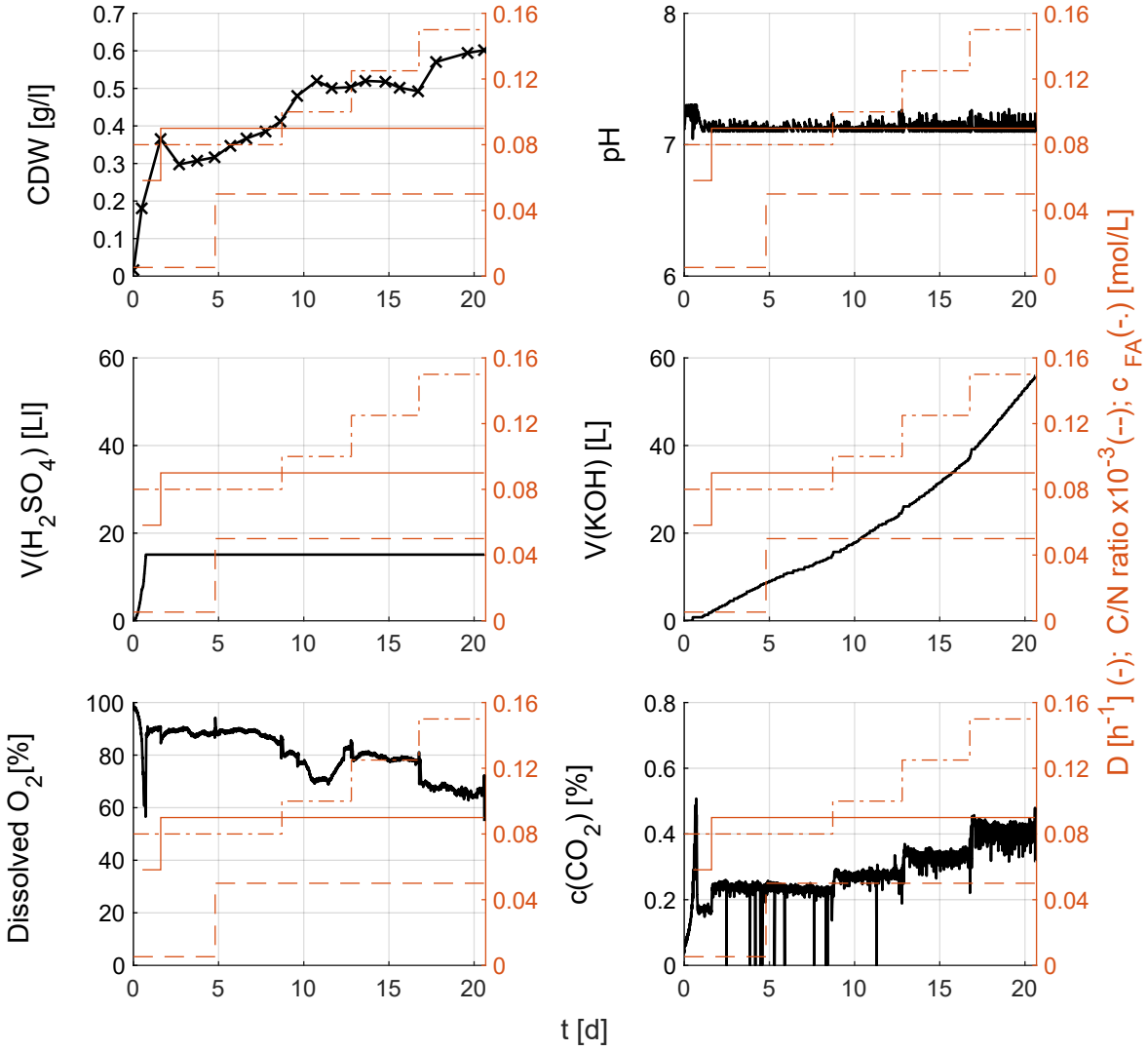

Figure S27. Biomass and online fermentation parameters during varying formic acid concentrations for PHB production of *C. necator* ALE26

To test PHB production in *C. necator* ALE26 under conditions of varying formic acid feed concentrations (-., dashed-dotted red line, secondary Y-axis), the organism was cultivated in

a 1 L chemostat culture. Samples were taken daily for offline biomass determination (CDW, top left). pH (top right), added volumes of acid and base (centre), dissolved oxygen (bottom left) and off-gas CO_2 concentrations (bottom right) were measured online through the ROSITA software. The C/N ratio (--, dashed red line, secondary Y-axis) was kept constant at 50 mol/mol (expressed as 0.05 mol/mol x 10-3 to scale with other parameters) for the entire nitrogen-limited phase of the experiment, while the dilution rate D remained at 0.09 h^{-1} (-, full red line, secondary Y-axis).

S12. Growth Profile of a Continuous Fermentation to Produce PHB in *C. necator* H16

For comparison with the adapted strain, *C. necator* H16 WT was cultivated in a separate chemostat. Initial fermentation parameters for the continuous phase were a dilution rate of 0.09 h^{-1}, C/N ratio of 50 mol/mol and 80 mM formic acid in the feed. Attempts at varying the C/N ratio by dropping the $(NH_4)_2SO_4$ concentration in the feed resulted in an unstable pH with large amounts of KOH and H_2SO_4 being added in a short time frame. Consequently, the biomass was almost washed out completely. After a reduction of the C/N ratio back to 50 mol/mol the chemostat recovered.

The recovered culture was then used to investigate the effect of different formic acid feed concentrations on the PHB accumulation capabilities of the WT strain.

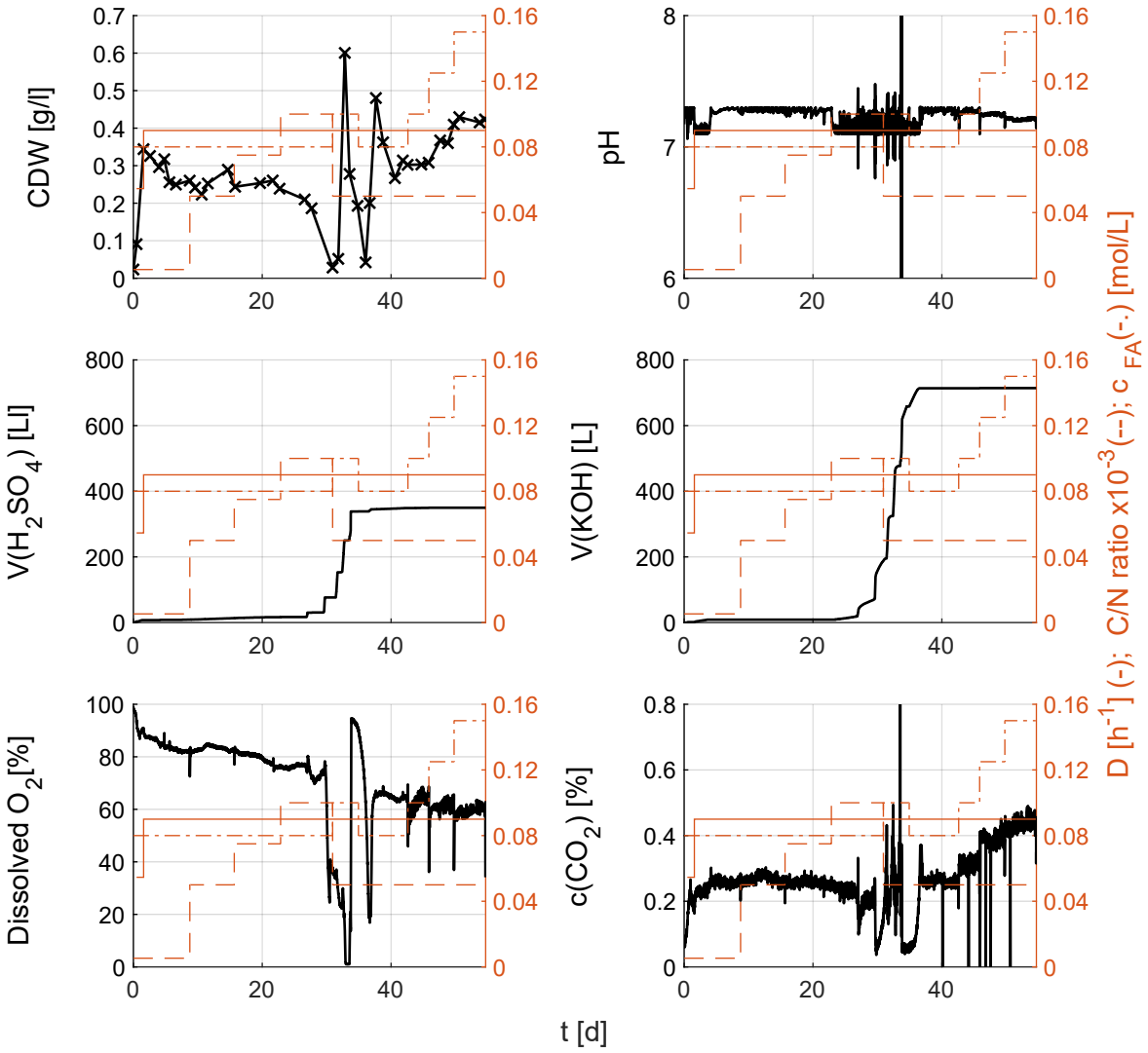

Figure S28. Biomass and online fermentation parameters during varying conditions for PHB production of *C. necator* H16

To test PHB production in *C. necator* H16 in varying conditions, the organism was cultivated in a 1 L chemostat culture. Samples were taken daily for offline biomass determination (CDW, top left). pH (top right), added volumes of acid and base (centre), dissolved oxygen (bottom left) and off-gas CO_2 concentrations (bottom right) were measured online through the ROSITA software. The C/N ratio (--, dashed red line, secondary Y-axis), dilution rate (-, full red line, secondary Y-axis) and formic acid concentration in the feed (-., dashed-dotted red line, secondary Y-axis) were varied over the course of the chemostat.

S13.1 PHB accumulation between C. necator *H16 and* C. necator *ALE26*

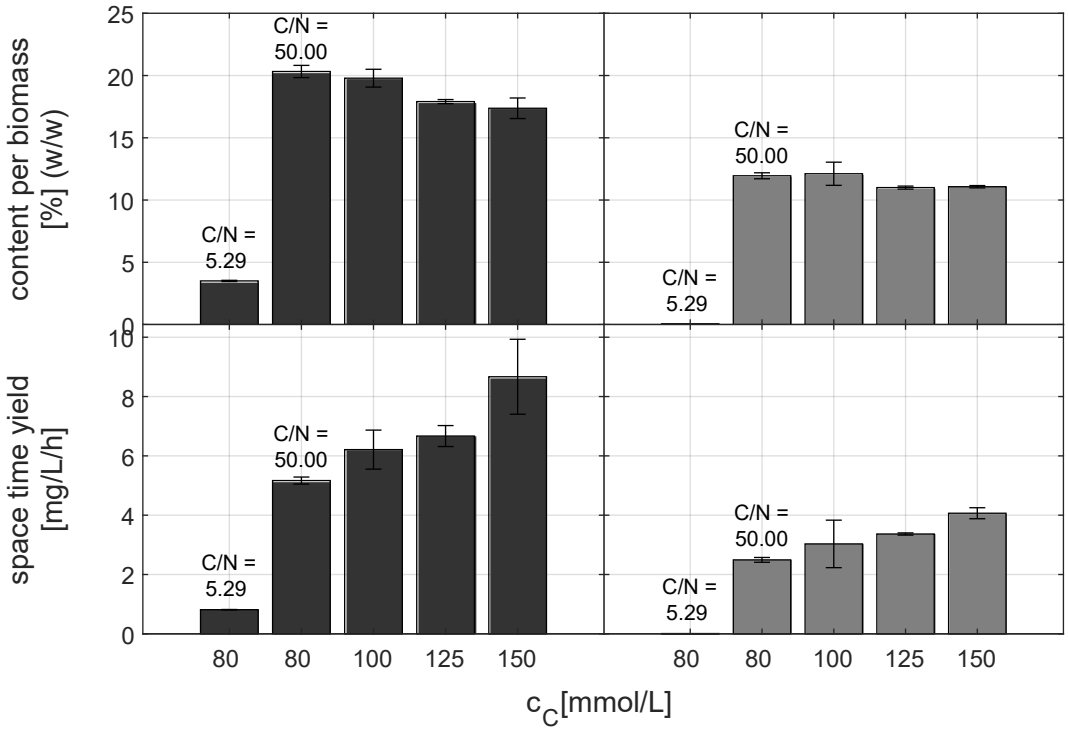

Figure S29. PHB content and space time yield of *C. necator* ALE26 (left) and H16 (right) under varying formic acid feed concentrations

PHB content of *C. necator* ALE26 (first column) and *C. necator* H16 (second column) was measured via GC from steady-state samples taken from continuous fermentations. The STY (Space Time Yield, i.e. concentration of the product per time) was calculated by taking into consideration the measured CDW of the freeze-dried pellets, the harvested volume and the dilution rate for each sample. All results were observed while keeping the dilution rate at 0.09 h^{-1} and the C/N ratio at 50 mol/mol, except for the first bar in each plot which resembles data in non-limited conditions. Error bars are representative of the standard deviation between two biological replicates.

The STY in batch cultivations was calculated using the following equation:

$$STY = \frac{\left(CDW\left[\frac{g}{L}\right] \times PHB\ content\left[\frac{g_{PHB}}{g_{CDW}}\right]\right)}{cultivation\ time\ [h]}$$

For continuous cultivations, instead the dilution rate was used:

$$STY = CDW\left[\frac{g}{L}\right] \times PHB\ content\left[\frac{g_{PHB}}{g_{CDW}}\right] \times D\left[h^{-1}\right]$$

S13. Growth and PHB Accumulation of *C. necator* ALE26 on $TBA.HCO_2$ (TBA.FA)

When sodium gluconate was supplied in the BioLector, addition of 2.5 mM and 10 mM TBA.FA slightly increased the final biomass, albeit with a longer lag phase and lower μ_{max}. At 20 mM however, growth was inhibited as the final biomass was almost six times lower than without any $TBA.HCO_2$. With 80 mM formic acid, additional $TBA.HCO_2$ up to 20 mM did not significantly alter the final biomass.

When $TBA.HCO_2$. was supplied as the sole carbon source, an increase in substrate concentration correlated with an increase in lag phase before growth could be observed. While in general the final biomass was higher with higher amounts of $TBA.HCO_2$, the lag phase on 80 mM substrate is almost four times as long as that on 40 mM. Still, growth was observed in all tested conditions.

The biomass yields on sodium gluconate were significantly higher than on the other substrates, consistent with what had been observed in comparative shake flask experiments for sodium gluconate and formic acid. While the μ_{max} of purely $TBA.HCO_2$ containing cultures was significantly lower than in those with formic acid, the final biomass between the two reached similar levels suggesting comparable carbon yields on the free acid and formate from the ammonium salt.

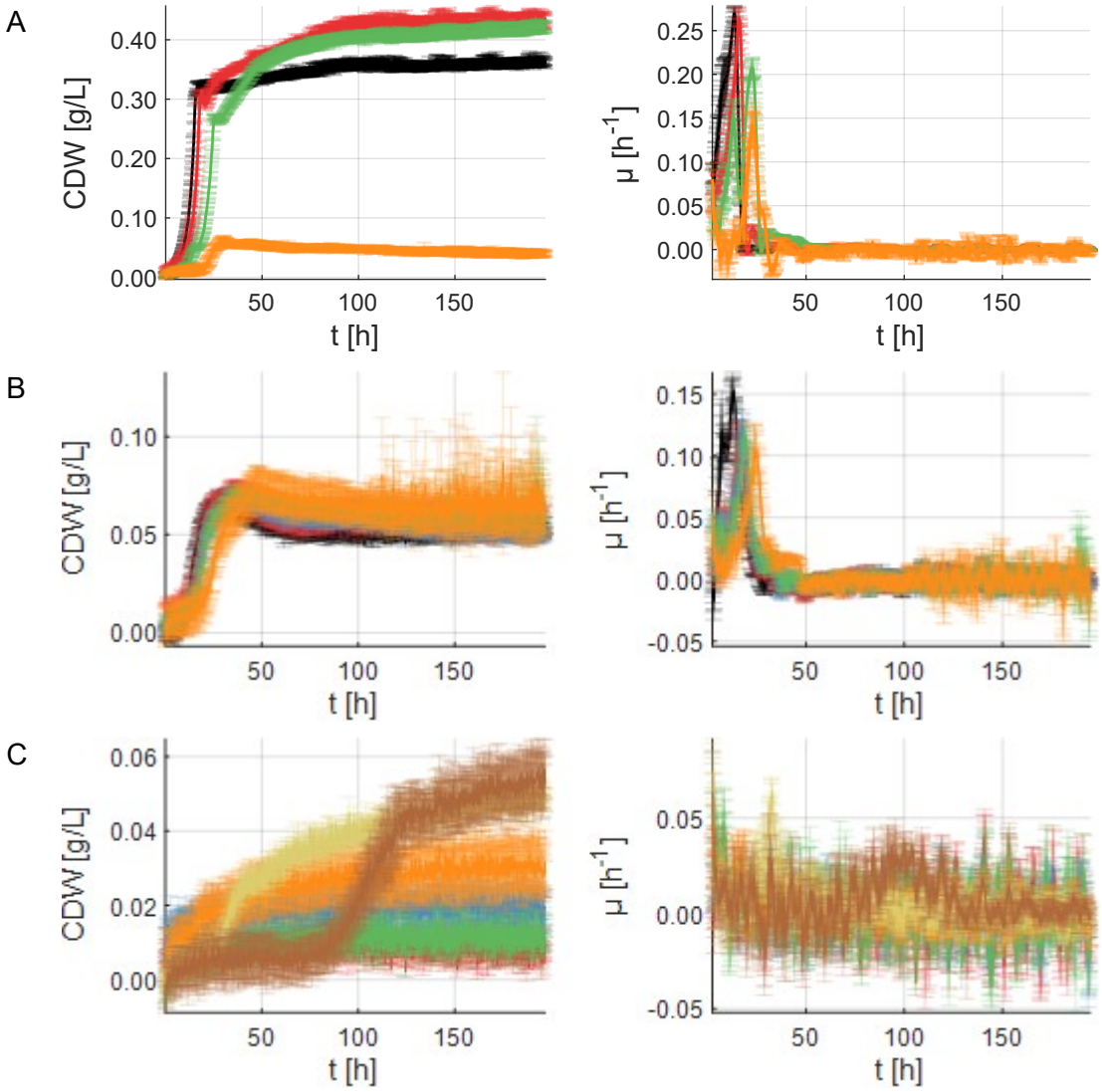

Figure S30. Growth curves of *C. necator* ALE26 on TBA.HCO_2

Growth of *C. necator* ALE26 was assessed in a BioLector on J-MM with various carbon source compositions. All conditions were tested in biological triplicates and growth rates calculated with a sliding window algorithm and a window size of 25 data points. Panel A shows cultures with 80 C-mM sodium gluconate supplemented with either no (black), 2.5 mM (red), 10 mM (green) or 20 mM (orange) TBA. TBA.HCO_2, panel B shows cultures with 80 mM formic acid supplemented with either no (black), 2.5 mM (red), 5 mM (blue), 10 mM (green) or 20 mM (orange) TBA.HCO_2 and panel C shows cultures with either 2.5 mM (red), 5 mM (blue), 10 mM (green) or 20 mM (orange), 40 mM (yellow) or 80 mM (brown) TBA.HCO_2 as the sole carbon source.

S14. PHB Production from $TBA.HCO_2$

C. necator ALE26 was cultivated in shake flasks to assess PHB accumulation on 40 mM $TBA.HCO_2$ in phosphate limitation to avoid the long lag phases encountered on 80 mM of the salt. Flasks with and without limitation were harvested after eight days and the pellets assessed for their PHB content. While the overall achieved biomass was significantly lower than on free formic acid, the organism accumulated 29.51 % (w_{PHB}/w_{CDW}) PHB to a final titer of 0.01 g/L (Figure S31). This percentage is equivalent to what was seen for cultivation on free formic acid under phosphate limitation. However, due to the almost eight-time longer growth and very low CDW on $TBA.HCO_2$, the final STY on this substrate is 0.052 mg/L/h. To provide enough biomass for PHB analysis, all triplicate samples were pooled into one, which is why no error is presented on this measurement.

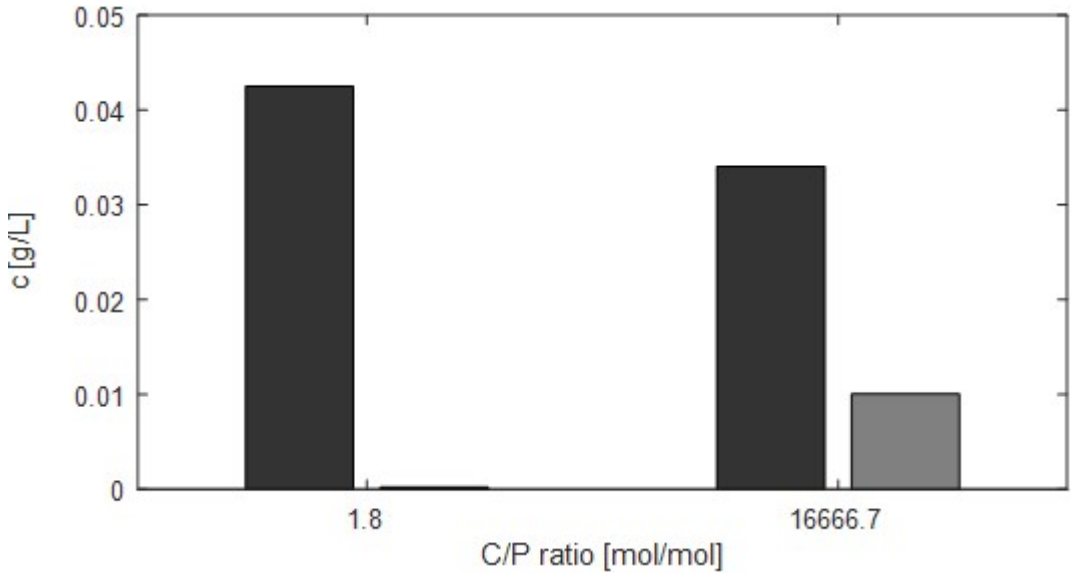

Figure S31. Biomass and PHB concentration for growth of *C. necator* ALE26 on $TBA.HCO_2$

PHB accumulation of *C. necator* ALE26 from 40 mM $TBA.HCO_2$ was assessed in batch cultivations in shake flasks. Biomass (dark grey) and PHB (light grey) concentrations were measured for carbon-limited growth (C/P ratio = 1.8) and under phosphate limitation (C/P ratio = 16666.7).

S15. Literature comparison

Table S6. Comparison of different CO_2 sources for PHB production using similar systems.

Entry	CO_2 source	Conditions	PHB STY [mg L^{-1} h^{-1}]	Ref.
1	CO_2 (diluted - 5 % CO_2) or industrial flue gas (3 – 6 % CO_2)	Photoautotrophic cultivation: Synechocystis UTEX 2973 [10 days and 21 da, pH=7, 38 °C]	> 3.02	[13]
2	Flue gas from a cogeneration plant (sparging at 25 mL/min)	Bioelectrochemical batch process: C. necator H16 [7 days, pH = 6.6, 30 °C]	1.98	[14]
3	Formate from electrosynthesis with pure CO_2	Biotransformation with resting cells: C. necator H16 [7.5 h, pH = 7.2, 30 °C]	8.40 [per OD_{600}]	[15]
4	Sodium formate from atmospheric air (0.04%CO_2)	Continuous cultivation: C. necator ALE26 [continuous, D = 0.09 h^{-1}, pH = 7.2, 30 °C]	6.34 ± 1.75	This work

S16. References

1. H. Li, P. H. Opgenorth, D. G. Wernick, S. Rogers, T.-Y. Wu, W. Higashide, P. Malati, Y.-X. Huo, K. M. Cho and J. C. Liao, *Science*, 2012, **335**, 1596-1596.

2. G. T. Little, M. Ehsaan, C. Arenas-López, K. Jawed, K. Winzer, K. Kovacs and N. P. Minton, *Microbiol Resour Announc*, 2019, **8**, e00814-00819.

3. D. Scheiner, *Water Research*, 1976, **10**, 31-36.

4. H. Brandl, R. A. Gross, R. W. Lenz and R. C. Fuller, *Appl Environ Microbiol*, 1988, **54**, 1977-1982.

5. R. G. Lageveen, G. W. Huisman, H. Preusting, P. Ketelaar, G. Eggink and B. Witholt, *Appl Environ Microbiol*, 1988, **54**, 2924-2932.

6. M. Jahn, N. Crang, M. Janasch, A. Hober, B. Forsström, K. Kimler, A. Mattausch, Q. Chen, J. Asplund-Samuelsson and E. P. Hudson, *eLife*, 2021, **10**, e69019.

7. P. G. Rouxhet and M. J. Genet, *Surface and Interface Analysis*, 2011, **43**, 1453-1470.

8. D. J. Morgan, *Surface and Interface Analysis*, 2015, **47**, 1072-1079.

9. I. Pollini, *Physical Review B*, 1994, **50**, 2095-2103.

10. F. M. by John and R. C. K. edited by Jill Chastain, Jr., *Handbook of x-ray photoelectron spectroscopy : a reference book of standard spectra for identification and interpretation of XPS data*, Eden Prairie, Minn. : Physical Electronics, [1995] ©1995, 1995.

11. S. M. Thalluri, J. Rodriguez-Pereira, R. Zazpe, B. Bawab, E. Kolíbalová, L. Jelinek and J. M. Macak, *Small*, 2023, **19**, 2300974.

12. E. Schwartz, A. Henne, R. Cramm, T. Eitinger, B. Friedrich and G. Gottschalk, *Journal of Molecular Biology*, 2003, **332**, 369-383.

13. H. Roh, J. S. Lee, H. I. Choi, Y. J. Sung, S. Y. Choi, H. M. Woo and S. J. Sim, *Bioresource Technology*, 2021, **327**, 124789.

14. A. Langsdorf, J. P. Schütz, R. Ulber, M. Stöckl and D. Holtmann, *Journal of CO2 Utilization*, 2024, **83**, 102800.

15. I. Dinges, I. Depentori, L. Gans, D. Holtmann, S. R. Waldvogel and M. Stöckl, *ChemSusChem*, 2024, **17**, e202301721.